Egypt. J. Chem. **Vol. 64,** No. 7 pp. 3767 - 3790 (2021)

Egyptian Journal of Chemistry

http://ejchem.journals.ekb.eg/

Optimized Synthesis of Biopolymer-Based Zinc Oxide Nanoparticles and Evaluation of Their Antibacterial Activity

Taha Farghaly Hassanein[a,*], Aya Samir Mohammed[a], Wael Sabry Mohamed[b], Rokaya Aly Sobh[b], Magdy Kandil Zahran[a]

[a] *Chemistry Department, Faculty of Science, Helwan University, Ain Helwan, Cairo 11795, Egypt*

[b] *Department of Polymers & Pigments, Chemical Industry Division, National Research Centre, Dokki, Giza 12622, Egypt*

Abstract

Owing to their unique properties, zinc oxide nanoparticles (ZnO NPs) have a broad range of exciting applications. However, the problem of nanoparticles aggregation remains challenging. So, biopolymers of polysaccharides can provide green and promising stabilizers as alternatives to the current toxic chemical stabilizers during ZnO NPs synthesis. The main idea in this investigation is to tune ZnO NPs with an appropriate texture, shape, and size for antibacterial application. So, this work compares the use of three different eco-friendly stabilizers namely starch, carboxymethyl cellulose, and hydroxyethyl cellulose as alternatives capping agents in the fabrication of ZnO NPs at various times. The optimized ZnO NPs sample was obtained using starch as the optimum stabilizer at reaction conditions of 0.5 h, room temperature (25 °C), 1:2 (M_{Zn}:M_{NaOH}) ratio and 1% (w/v) starch concentration. The optical, texture, and structural properties of prepared ZnO NPs were characterized by UV−Vis, DLS, zeta potential, FT-IR, and TEM techniques. ZnO NPs showed a mean zeta potential of −21.6 mV, explaining that they are moderately stable. The analysis by TEM confirmed that the NPs were spherical and have an average size of 23 nm. The antibacterial properties of ZnO NPs against Gram-positive (*Bacillus subtilis* and *Staphylococcus epidermidis*) and Gram-negative (*Enterobacter cloacae* and *Escherichia coli*) bacteria were evaluated based on the zone of inhibition (ZOI) values expressed in mm. The results showed promising performances for their antibacterial activity against the tested bacteria which indicated a strong antibacterial activity of ZnO NPs against *B. subtilis*, *S. epidermidis*, and *E. cloacae* with ZOI values of 17, 14 and 16 mm, respectively, and it showed moderate activity against *E. coli* (ZOI = 10 mm). The synthesis of biopolymer stabilized ZnO NPs by this approach could be eco-friendly and cost-effective and synthesized ZnO NPs can serve as promising antibacterial agents.

Keywords: ZnO nanoparticles; Biopolymer; Polysaccharides; Starch; Cellulose; Antibacterial

1.Introduction

The infectious diseases caused by bacterial contamination pose a serious threat to human health in many sectors including environmental, packaging, food, textile as well as hospital and medical care. To stop the spreading of the diseases, the development of antibacterial agents derived from metal oxides and cellulose-based nanomaterials has attained a growing interest in recent years [1-4]. Metal oxides nanomaterials with antibacterial properties when encapsulated or coated onto surfaces can meet extensive applications in water treatment, packaging, coating, wound healing, and the biomedical field [1, 5]. Among the antibacterial nanoscale metal oxides, zinc oxide nanoparticles (ZnO NPs) are one of the most promising antibacterial agents due to their unique properties and non-toxic nature [1, 6]. Moreover, zinc oxide is currently regarded as generally recognized as a safe (GRAS) substance by the US Food and Drug Administration (FDA) [6]. Recently, ZnO NPs have earned a strong consideration because of their exclusive chemical, physical, and biological properties that make these

*Corresponding author e-mail: taha1m@yahoo.com
Received date: 08 May 2021; revised date 11 June 2021; accepted date 13 June 2021
DOI: 10.21608/EJCHEM.2021.75677.3709

NPs suitable for a vast range of applications in various areas of industry, medicine, agriculture, food, electronics, and environmental remediation [7-10].

Most markedly, ZnO NPs find applications in biological labeling, bio-sensing, drug delivery, and nanomedicine due to their anti-inflammatory, antiseptic, anticancerous activity, wound healing ability, and antibacterial effectiveness against different pathogens [11] and multidrug-resistant bacteria [12]. The mentioned properties and applications can be tuned by the optimized synthesis of ZnO NPs because it has been observed that the properties of ZnO NPs are strongly dependent on the size, morphology, synthesis method, and varying conditions during processing [13]. Also, some other factors should be considered such as high speed, simplicity, eco-friendly, and low cost of their preparation.

Several techniques for the synthesis of ZnO NPs have been reported in the literature such as precipitation [13, 14], hydrothermal [8, 15], solvothermal [16], green synthesis [10, 13], sol-gel [12, 17], and chemical vapor deposition [18]. Among the aforementioned synthetic routes, precipitation is the prominent and most effective method because it offers many advantages such as simplicity, low cost, and high yield [19-22]. Moreover, precipitation does not need complicated equipment.

Maintaining the stability of ZnO NPs is an essential prerequisite for their application since nanoparticles tend to agglomerate easily due to their high surface energies. The simplest method of stabilizing is by a surface coating surrounding the particles; this reduces the interaction between the nanoparticles; thereby inhibiting its aggregation [23]. Several reports have been articulated the use of many conventional chemical stabilizers such as functionalized long-chain hydrocarbons, polymers, block copolymers, and dendrimers [7, 24, 25]; their major drawback is primarily the use of highly toxic solvents or chemicals that are unsafe to the environment. So, green materials were introduced as several bioinspired methods for the synthesis of nanomaterials recommending the use of bio-origins such as enzymes, vitamins, polyphenols, phytochemicals, and polysaccharides (starch, chitosan, cellulose, etc.) [2-4, 7, 26].

Biopolymers are greener and safer materials that comply with the principles of green chemistry. Due to their abundance, cost-effectiveness, biocompatibility, and unique properties, biopolymers such as starch [27] and cellulose derivatives [1, 28] are very promising materials for use as stabilizers in the preparation of ZnO NPs under the safest and greenest conditions. Also, these types of stabilizers can reduce agglomeration among the smaller ZnO NPs through many O-H functional groups contained in their chemical structures that can interact with nanoparticles surfaces at the initial nucleation step. Here also starch and cellulose derivatives can play a dual role as a capping agent and functionalizing agent which is very useful in the various applications of ZnO NPs [27, 28].

Herein, ZnO NPs were synthesized in the present research via a wet chemical precipitation reaction in the presence of a biopolymer stabilizing agent. An attempt has been made in this investigation to optimize the method to get the optimum reaction conditions to obtain the possible smallest particle size and proper morphology that can enhance the antibacterial efficiency [5, 11]. Hence, $ZnSO_4.7H_2O$ (as a zinc salt precursor) is used separately in the presence of one stabilizer: starch, or carboxymethyl cellulose (CMC), or hydroxyethyl cellulose (HEC) at various times. Other synthesis conditions such as temperature, Zn salt to NaOH molar ratio, and stabilizer concentration were varied during ZnO NPs synthesis using the best stabilizer. Noticeably, in literature, few experimental studies are investigating the synthesis of ZnO NPs at different synthetic conditions using polysaccharides biopolymers. According to our knowledge, the application of both CMC and HEC as capping agents for ZnO NPs is scarce. The synthesized ZnO NPs are characterized by techniques such as UV–Vis, DLS, zeta potential, FT-IR, and TEM. Further, the antibacterial activity of ZnO NPs was examined against Gram-positive (*Bacillus subtilis* (*B. subtilis*) and *Staphylococcus epidermidis* (*S. epidermidis*)) and Gram-negative (*Enterobacter cloacae* (*E. cloacae*) and *Escherichia coli* (*E. coli*)) bacteria by the agar well diffusion technique.

2. Materials and Methods

2.1. Materials

The materials used (purity, Supplier Company, town, country) for ZnO NPs synthesis are summarized in Table 1. The chemical structures of starch, CMC, and HEC used as stabilizers are given in Fig. 1. The microorganisms tested for the evaluation of the antibacterial efficacy of synthesized ZnO NPs were collected from the Regional Center for Mycology and Biotechnology (RCMB), Faculty of Science, Al-Azhar University, Cairo, Egypt. The examined bacteria were: Gram-positive (*B. subtilis* (RCMB 015) and *S. epidermidis* (RCMB 009)) and Gram-negative (*E. cloacae* (RCMB 001) and *E. coli* (RCMB 010052)). DMSO (ACS reagent grade, 99.9%), used in antibacterial tests, was supplied by Sigma Aldrich Chemie GmbH (Taufkirchen, Germany).

Table 1. Materials used in the synthesis of ZnO NPs.

Materials	Purity % (w/w)	Supplier Company	Town	Country
Zinc sulfate heptahydrate ($ZnSO_4.7H_2O$)	99	El-Nasr Pharmaceutical Chemicals	Cairo	Egypt
Sodium hydroxide (NaOH)	97	El-Nasr Pharmaceutical Chemicals	Cairo	Egypt
Starch	99	Biotech	Cairo	Egypt
Carboxymethyl cellulose sodium salt (CMC)	≥ 99.5	Janssen Pharmaceuticals	Brussel	Belgium
Hydroxyethyl cellulose (HEC)	≥ 99.5	The Dow Chemical	Midland	USA

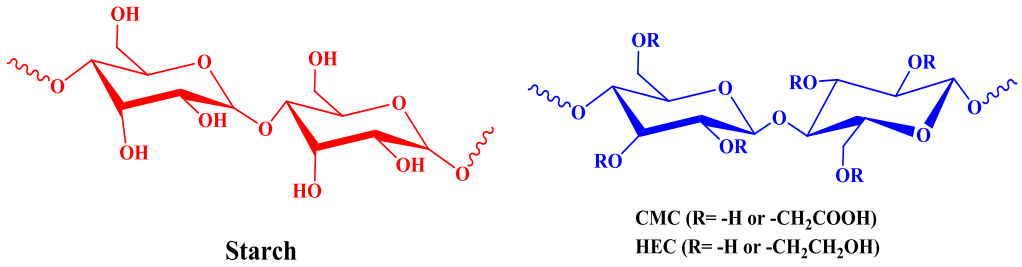

Fig. 1. Chemical structures of starch, CMC, and HEC biopolymers stabilizers.

2.2.Synthesis of ZnO NPs

Zinc oxide nanoparticles (ZnO NPs) were synthesized by the wet chemical precipitation reaction between $ZnSO_4.7H_2O$ and NaOH in the presence of a biopolymer stabilizing agent. To obtain the optimum ZnO NPs sample, $ZnSO_4.7H_2O$ is used separately in the presence of one stabilizer (starch, or CMC, or HEC) according to the various synthesis conditions that are summarized in Table 2.

In a typical synthesis procedure, separate solutions of $ZnSO_4.7H_2O$, NaOH, and a stabilizer were prepared and stirred vigorously at 900 rpm using a MS300 magnetic stirrer (Shanghai Leewen Scientific Instrument Co., Ltd, Shanghai, China) till complete dissolution. An aqueous solution of stabilizer was then mixed with the zinc salt solution, and the mixture was magnetically stirred at 750 rpm until a homogeneous solution was obtained. Afterward, the prepared NaOH solution was added drop by drop to this mixture solution, with steady stirring (750 rpm). Stirring was continued for a determined time (Table 2) after the complete addition of NaOH solution; a white precipitate was formed.

After fulfilment of the reaction, the solution mixture was left overnight for ageing of the precipitate. The obtained supernatant liquid was discarded carefully. The settled white precipitate was separated from the solution by centrifugation (10000 rpm for 10 min; Centurion Scientific Ltd, C2 series, West Sussex, UK) and was washed five times with deionized water using a Q125 probe sonicator (Qsonica, Newtown, USA) and centrifugation devices. Washing was carried out to remove unreacted materials, impurities and to remove any possible absorbed ions and chemicals by the precipitate to reduce agglomeration. The derived precipitate was then dried using a laboratory oven at 80 °C overnight and subsequently, the product was crushed into a fine powder. The ZnO NPs were readily obtained by calcination of the dried powder at 400 °C for 2 h using a muffle furnace (Thermolyne MF-8020, Gilson Co., Inc., Lewis Center, USA). During ZnO NPs synthesis, some parameters such as time, temperature, salt to NaOH molar ratio, and stabilizer concentration were varied (Table 2). The synthetic procedure steps for ZnO NPs are briefly summarized in Fig. 2.

2.3. Characterization of ZnO NPs

The optimum ZnO NPs samples at various synthesis conditions were determined based on their UV-Vis absorption peaks and confirmed using dynamic light scattering (DLS) analysis for particle size. Other characterizations such as FT-IR, zeta potential, and transmission electron microscopy (TEM) analysis were performed only on the best optimum ZnO NPs sample.

2.3.1. UV–Vis spectral analysis

The UV-Vis absorption peaks of ZnO NPs were reported using a UV-Vis spectrophotometer (JASCO, V-630, Portland, OR, USA) at room temperature in the scanning wavelength region of 200 - 800 nm. The ZnO NPs powder samples were dispersed in deionized water and their absorbance was analyzed using a 1 cm quartz cell. The samples were well sonicated before measurement, for uniform dispersion.

2.3.2. FT-IR spectrum

The composition of ZnO NPs was characterized by the FT-IR spectroscopy within the 400-4000 cm-1 wavenumber range using Alpha FT-IR spectrophotometer (Bruker, Billerica, Massachusetts, USA) which is equipped with an ATR sample base plate Diamond.

Table 2. Synthesis conditions detail of ZnO NPs using starch, CMC, and HEC.

Stabilizer	Time (h)	Temperature (°C)	M_{Zn}:M_{NaOH}	Stabilizer concentration (w/v %)	Corresponding UV-Vis Figure
Starch	0.5	25	1:2	1	Fig. 3a
Starch	2	25	1:2	1	Fig. 3a
Starch	6	25	1:2	1	Fig. 3a
Starch	18	25	1:2	1	Fig. 3a
CMC	0.5	25	1:2	1	Fig. 3b
CMC	2	25	1:2	1	Fig. 3b
CMC	6	25	1:2	1	Fig. 3b
CMC	18	25	1:2	1	Fig. 3b
HEC	0.5	25	1:2	1	Fig. 3c
HEC	2	25	1:2	1	Fig. 3c
HEC	6	25	1:2	1	Fig. 3c
HEC	18	25	1:2	1	Fig. 3c
Starch	0.5	50	1:2	1	Fig. 4
Starch	0.5	70	1:2	1	Fig. 4
Starch	0.5	25	1:1	1	Fig. 5
Starch	0.5	25	1:3	1	Fig. 5
Starch	0.5	25	1:4	1	Fig. 5
Starch	0.5	25	1:2	0	Fig. 6
Starch	0.5	25	1:2	3	Fig. 6
Starch	0.5	25	1:2	5	Fig. 6

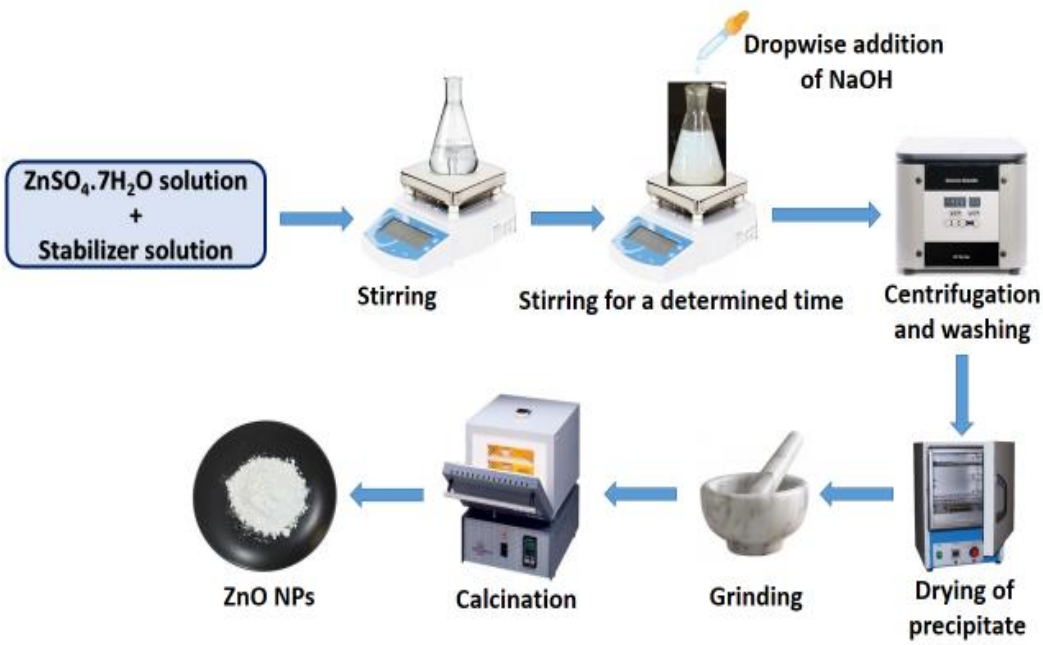

Fig. 2. Synthetic procedure steps for ZnO NPs.

2.3.3. DLS for particle size analysis

The average size for ZnO NPs dispersed in deionized water has been analyzed at 25 °C using DLS technique using a Malvern Zetasizer 2000 (Nano-ZS; Malvern Instruments, Malvern, UK). Nanoparticles were suspended in deionized water by applying sonication before each measurement.

2.3.4. Measurement of zeta potential

The zeta potential (ζ-P) of nanoparticles is a principal factor for the stability of the suspended particles. Hence ζ-P was determined using a Malvern Zetasizer 2000 (Nano-ZS; Malvern Instruments, Malvern, UK) using the Laser Doppler Velocimetry (LDV) technique. A freshly prepared amount of ZnO NPs was placed into a disposable folded capillary zeta cell at 25 °C and 13° scattered angle.

2.3.5. TEM analysis

The texture of ZnO NPs was examined by TEM analysis using a JEOL JEM-2100 electronic microscope (JEOL, Ltd., Tokyo, Japan) with an accelerating voltage of 100 kV. Specimens for TEM measurements were prepared by depositing a droplet of ZnO NPs suspension on carbon-coated film (400 mesh) copper grid after which the solvent was evaporated in the air at 25 °C.

2.4. Antibacterial activity evaluation of ZnO NPs

Antibacterial activity assay was performed by the agar well diffusion technique [29] which has been the most as often as possible utilized methods; standardized as an official technique for detecting the bacteriostatic activity. The antibacterial activity of ZnO NPs was investigated against two Gram-positive (B. subtilis and S. epidermidis) and two Gram-negative (E. cloacae and E. coli) bacteria. A sterilized stainless steel cork borer was used to cut wells with 6 mm diameter in the agar plates. A 100 µl (10 mg/ml) of ZnO NPs (suspended in DMSO) was then poured into the wells. Suspended ZnO NPs samples were sonicated for 15 min before loading into the wells. In positive control, Ciprofloxacin (5 µg/ml) and Gentamicin (4 µg/ml) were used as standard drugs against Gram-positive and Gram-negative bacterial strains, respectively; whereas negative control was 100 µl of DMSO free of nanoparticles. All the agar plates were incubated for 24 h at 37 °C. The diameters of clear zones of inhibition (ZOI) formed around the wells were then measured and expressed in mm. All the tests were performed under sterile conditions in triplicate. The ZOI values were presented as mean ± SD for three measurements.

3. Results and discussion

3.1. Optimization of ZnO NPs synthesis

To obtain the optimum ZnO NPs, firstly, two factors were investigated: type of stabilizer and reaction time (Table 2). The optimum ZnO NPs samples at various synthesis conditions (Table 2) were determined based on some parameters such as UV-Vis absorption peaks and zetasizer DLS measurements.

3.1.1. Synthesis of ZnO NPs using different stabilizers at various time

The progressive production of ZnO NPs was identified by UV-Vis spectroscopy, which has confirmed to be a helpful spectroscopic technique for the detection of the formulation of NPs over time. Fig. 3 shows UV-Vis absorption spectra of prepared ZnO NPs using different stabilizers (starch, CMC, and HEC) at various reaction times: 0.5 h, 2 h, 6 h, and 18 h. The absorbance band characteristics of ZnO NPs stabilized by starch, CMC and HEC were detected in the range of 346–341 nm, 375–357 nm, and 352–341 nm, respectively, with the increase in reaction time from 0.5 h to 18 h (Fig. 3). The λmax values of ZnO NPs are also summarized in Table 3. The ZnO NPs characteristic peak was centered at around 350 nm which is a characteristic peak of ZnO NPs. This value suggests that the ZnO NPs were spherical and have been verified by the TEM analysis of this research. Previous results have indicated that the spherical ZnO NPs assign to the absorbance bands at about 350 nm in the UV–Vis spectra [30].

Table 3. The λ_{max} values (nm) of ZnO NPs synthesized using starch, CMC, and HEC as stabilizers at various reaction times.

Time (h)	λ_{max} values (nm)		
	Starch	CMC	HEC
0.5	346	375	352
2	342	366	350
6	342	358	348
18	341	357	341

As shown in Fig. 3a, the absorbance peak is slightly blue-shifted to 342 nm when the time reached 2 h, after which the λ_{max} value was not changed with the increase in reaction time to 18 h.

By increasing the reaction time to 2 h and 6 h (Fig. 3b), the absorbance peaks are blue-shifted to 366 and 358 nm, respectively. Further increase in time from 6 h to 18 h does not cause any noticeable change in λ_{max} value. A small blue shift (from 352 to 348 nm) was also observed when the reaction time varied from 0.5 h to 6 h (Fig. 3c). Moreover, with the increase in reaction time to 18 h, the absorbance band was also blue-shifted to 341 nm. Blue-shift was reported by Darroudi et al. [31] for the colloidal Ag-NPs prepared using glucose as a stabilizer at various synthesis times; the λ_{max} value was blue-shifted from 440 nm to 430 nm with the increase in reaction time from 1 h to 48 h. These results were also in an agreement with Venditti et al. [32] reported that the surface plasmon resonance (SPR) peak is blue-shifted from 554 nm to 527 nm when the time increased from 2 h to 24 h.

Generally, the absorbance bands are affected by the shape, size, and morphology of the prepared nanoparticles [32-34]. A blue shift in the wavelength of the peak indicating a progressive growth of ZnO NPs with increasing the time of reaction and the improvement of the stabilization process promoted by the stabilizer that leads to the formation of smaller nanoparticles. It has an agreement with the Mie theory predicted when the size of nanoparticles decreases, a blue-shift of SPR peak position would be seen [35]. So, there is a strong relationship between the absorption peak of ZnO NPs caused by SPR and their sizes.

The comparison between the absorption peaks of ZnO NPs prepared using starch, CMC, and HEC stabilizers (Fig. 3a–c) and its λ_{max} values reported in Table 3 indicated that ZnO NPs stabilized with starch are the NPs obtained with the smallest size within a short reaction time (0.5 h). This is also consistent with further DLS characterizations (see below). So, all subsequent experiments for ZnO NPs synthesis at other different conditions were performed using starch as a stabilizer.

3.1.2. Synthesis of ZnO NPs using starch as a stabilizer at different operating parameters

It is concluded from the previous section that the optimum ZnO NPs sample is the one prepared using starch as a stabilizer for 0.5 h of reaction. The present section has demonstrated the systematic studies on ZnO NPs synthesis controlled by different reaction parameters including; reaction temperature, Zn salt to NaOH molar ratio (M_{Zn}:M_{NaOH}) and starch concentration. During the evaluation of a specific reaction parameter, other reaction conditions were fixed. Understanding the effect of these parameters is very useful in the preparation of ZnO NPs by this technique due to the properties of these nanoparticles depend greatly on their size and morphology [36]. The main idea in this investigation is to form ZnO NPs with an appropriate texture, shape, and size for the intended application.

3.1.2.1. Effect of temperature

The temperature of the reaction is an interesting factor that affects both the textural properties and the size of the prepared particles [37]. Fig. 4 shows UV-Vis spectra of the ZnO NPs synthesized using starch at various reaction temperatures: 25 °C, 50 °C, and 75 °C.

It is seen that, at temperature 25 °C, the maximum absorption peak is observed at 346 nm. Increasing the preparation temperature to 50 °C and 75 °C resulted in a red shift towards higher absorption bands of 358 and 376 nm, respectively. This red shift can be attributed to the agglomerations in the samples under the influence of higher temperatures [38]. According to the Mie theory model, red-shifts are observed as size increased [35]. So, the size of ZnO NPs increased as the reaction temperature increased. On heating, when the particles are produced, they strike and either combine with one another to form a bigger particle or agglomerate; the process which depends upon the reaction temperature and the energy gained by the particles; and so the particle size increased with increasing temperature [37]. This is consistent with the study reported by Jyoti et al. [37] for the synthesis of ZnO NPs which indicated that the particle size increases with the rising reaction temperature.

3.1.2.2. Effect of Zn salt to NaOH molar ratio (M_{Zn}:M_{NaOH})

Various researchers [37, 39-42] suggested that Zn salt and/or NaOH concentrations play a crucial role in the obtained size, texture, and optical properties of ZnO nanostructures. The UV-Vis absorbance peaks of ZnO NPs prepared at various Zn salt to NaOH molar ratio (M_{Zn}:M_{NaOH}) from 1:1 to 1:4 are depicted in Fig. 5.

Obviously, at M_{Zn}:M_{NaOH} of 1:1, there is an absorption peak observed at 341 nm. By decreasing M_{Zn}:M_{NaOH} to 1:2, the absorption peak is slightly red-shifted to 346 nm. On decreasing the M_{Zn}:M_{NaOH} further to 1:3 and 1:4, the absorption peaks are highly red-shifted to 358 and 375 nm, respectively. This could be attributed to the formation of larger particles; the particle size increased with the decrease in the M_{Zn}:M_{NaOH} from 1:1 to 1:4 (or increase of NaOH concentration from 0.1 M to 0.4 M).

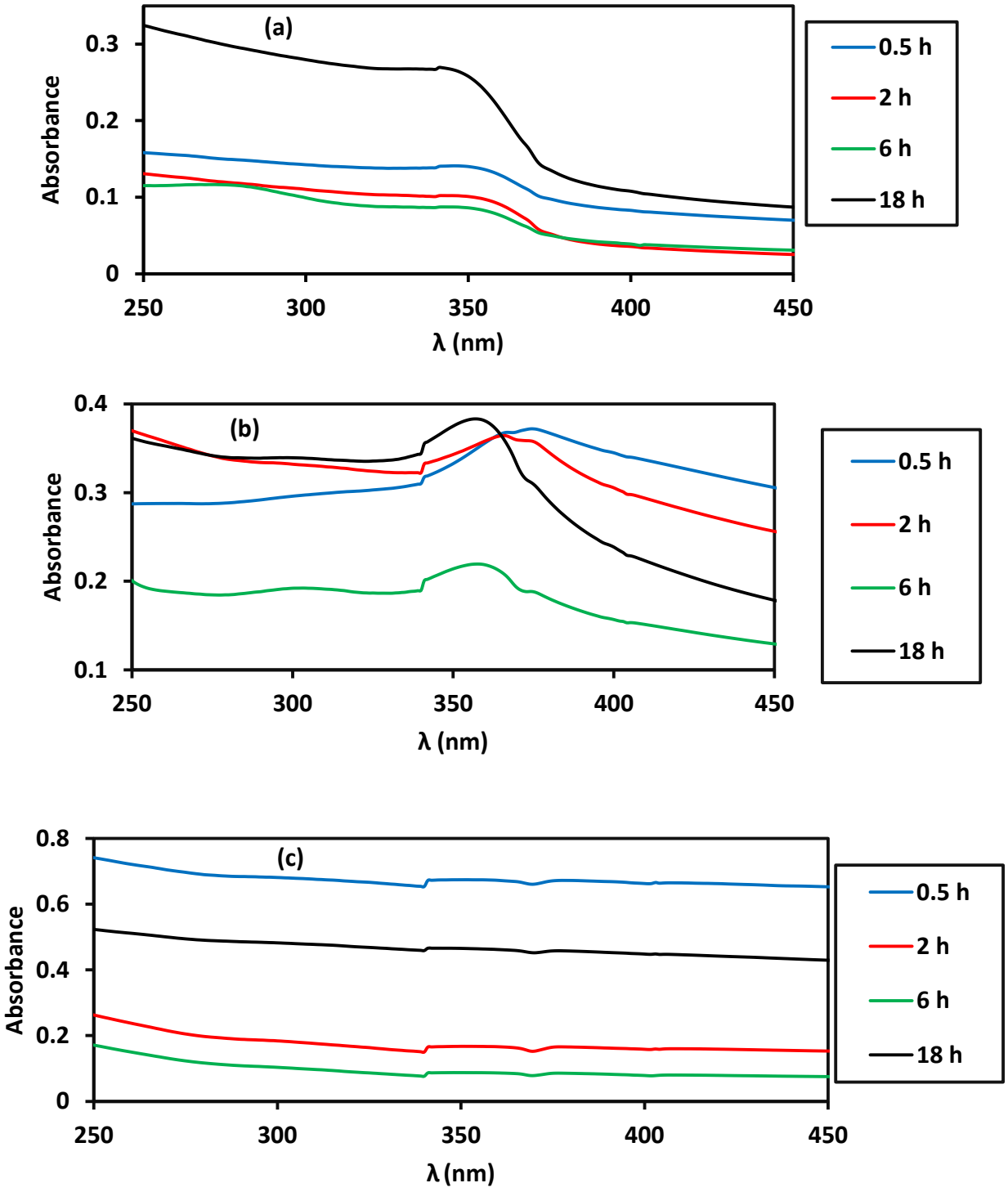

Fig. 3. UV-Vis absorption spectra of ZnO NPs synthesized using different stabilizers (a) starch, (b) CMC and (c) HEC at various reaction times (temperature: 25 °C; M_{Zn}:M_{NaOH} = 1:2; stabilizer concentration: 1%).

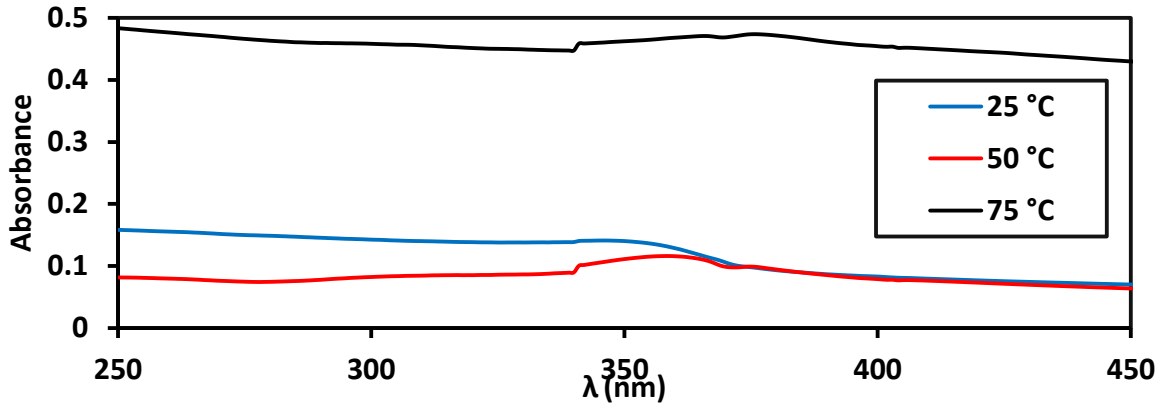

Fig. 4. UV-Vis absorption spectra of ZnO NPs synthesized using starch at different temperatures (time: 0.5 h; M_{Zn}:M_{NaOH} = 1:2; starch concentration: 1%).

The survey of many significant reports [37, 40, 41, 43, 44] declares that the size of ZnO NPs is in direct proportionality to the NaOH concentration; accordingly, the particle size increases. With the increase in NaOH molar concentration, the reaction rate also increases and so there is a better chance for the production of $Zn(OH)_2$ nuclei and the growth of the crystals consequently. This increase in particle size with increasing NaOH concentration is also based on Ostwald ripening phenomenon [41, 45] in which the small ZnO particles are being consumed as the larger ones grow bigger; this happens because bigger particles are more energetically favored than smaller particles.

The increase of size with the decrease of M_{Zn}:M_{NaOH} (or increase of NaOH concentration) can also be interpreted based on Gibb's free energy, ΔG, corresponded with the NPs [37, 46]. The driving force for both nucleation and growth is the reduction of ΔG. The change of ΔG is dependent on the concentration of the solute [37, 46]:

$$\Delta G = - KT/\Omega \ln(C/C_0) \quad (1)$$

Where K: is Boltzmann's constant, T: is the temperature, C: is the solute concentration, C_0: is the concentration at equilibrium or solubility, Ω: is the atomic volume. It is concluded from the above relation that ΔG increases as the concentration increases. For this energy to be lower, the growth of particles continues if the smallest energy needed for the stability of particles is not achieved [37]. So, the particles acquire the size in this way so as to diminish ΔG. When the concentration of OH^- increases, ZnO NPs would growing faster than they nucleate, more easily aggregate, results in larger particles.

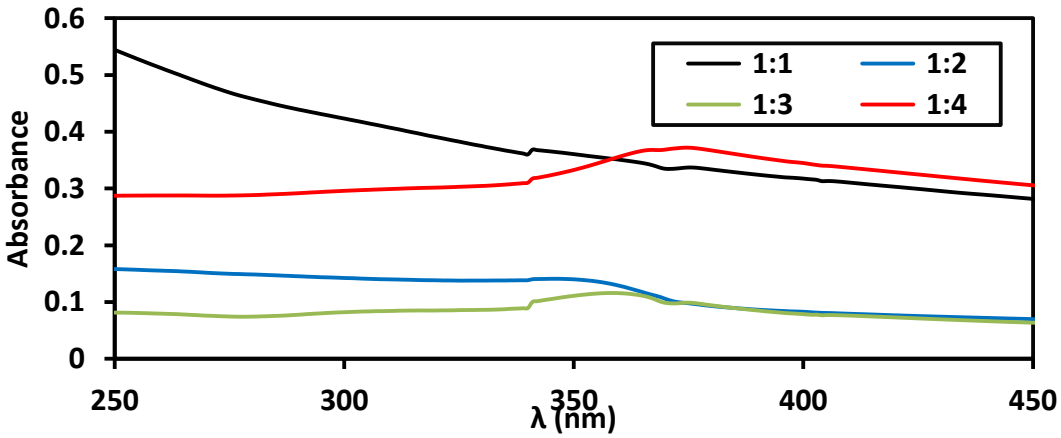

Fig. 5. UV-Vis absorption spectra of ZnO NPs synthesized using starch at different M_{Zn}:M_{NaOH} ratio (time: 0.5 h; temperature: 25 °C; starch concentration: 1%).

The results in our approach are consistent with those reported by Jyoti et al. [37] when NaOH concentration increased from 2 M to 10 M, the particle size of ZnO NPs increased. A study cited by Nath et al. [40] further reveals increasing in crystallite size of ZnO NPs from 20 nm to 50 nm with the increase in NaOH concentration from 2.5 M to 7.5 M which is confirmed by field emission scanning electron microscopy. Although the red shift was observed with the change of the molar ratio from 1:1 to 1:2, the optimum molar ratio selected was 1:2 for the formation of ZnO NPs; under stoichiometric conditions (1:2 ratio) higher yield of ZnO NPs are produced. Also, the size of ZnO NPs using a 1:2 molar ratio still in the nano-scale as confirmed from both DLS (68.43 nm) and TEM (23 nm) characterizations (see below).

3.1.2.3. Effect of starch concentration

The influence of starch concentration (0-5% (w/v)) on the UV-Vis absorption spectra for ZnO NPs was investigated and demonstrated in Fig. 6. Without using starch (0%), the λ_{max} obtained was 373 nm. When starch is added to zinc sulfate solution with 1% concentration, the λ_{max} changed significantly to 346 nm. Further increase in starch concentration to 3 % and 5 % does not cause a significant change in λ_{max} value. As noted from the blue shift as the starch concentration increased (Fig. 6), the size of ZnO NPs prepared without starch was much larger than those prepared with starch stabilizer. The UV-Vis data was also confirmed with DLS results (see below). Due to the high polarity of water, ZnO NPs cause an immediate agglomeration during synthesis without a protective agent with water due to the Vander wall forces of attraction [47]. To prevent agglomeration, soluble starch has been used as a stabilizer, which played a great role in the synthesis and stabilization of ZnO NPs (see section 3.2).

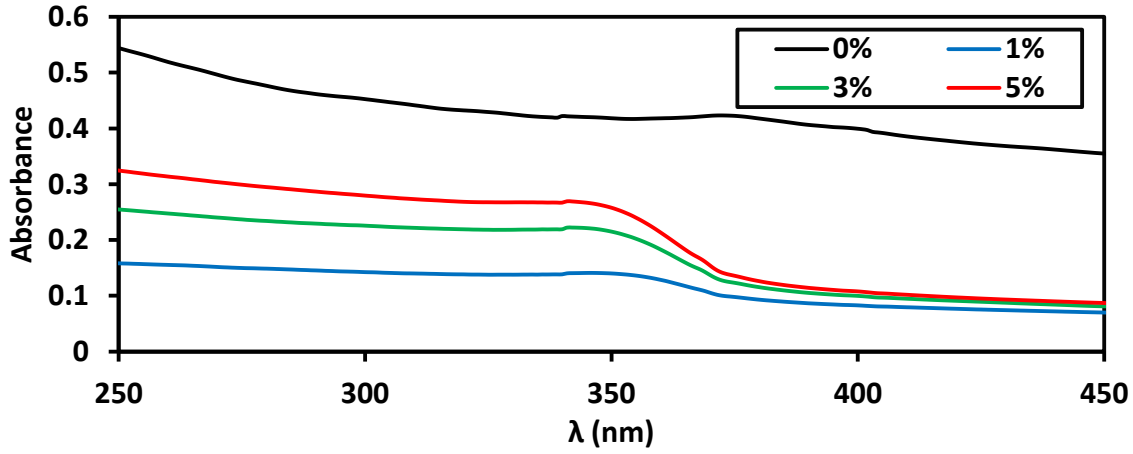

Fig. 6. UV-Vis absorption spectra of ZnO NPs synthesized using starch at different starch concentrations (time: 0.5 h; temperature: 25 °C; M_{Zn}:M_{NaOH} = 1:2).

3.2. Mechanism of ZnO NPs formation and stabilization

The chemical reactions governing ZnO NPs formation in the absence of stabilizer can be summarized as follows:

1. When $ZnSO_4.7H_2O$ salt is dissolved in deionized water, it is dissociated into its ions and so Zn^{2+} ions are formed:
$$ZnSO_4 \rightarrow Zn^{2+}+SO_4^{2-} \quad (1)$$
2. Upon addition of NaOH, pH increases to about 10-12, and the unstable compound $Zn(OH)_2$ is precipitated:
$$Zn^{2+}+2OH^- \rightleftharpoons Zn(OH)_2 \quad (2)$$
3. In excess of NaOH, the zinc hydroxide precipitate will dissolve, therefore, a colorless solution of zincate ions ($Zn(OH)_4^{2-}$) complexes will produce, which serve as basic growth units for the synthesis of ZnO NPs [48]:
$$Zn(OH)_2+2OH^- \rightleftharpoons Zn(OH)_4^{2-} \quad (3)$$
4. ZnO NPs production by dehydrating of $Zn(OH)_4^{2-}$:
$$Zn(OH)_4^{2-} \rightarrow ZnO+H_2O+2OH^- \quad (4)$$

The overall chemical reaction governing the formation of ZnO is as follows:

$$ZnSO_4.7H_2O + 2NaOH \rightarrow ZnO + Na_2SO_4 + 8\ H_2O \quad (5)$$

In equation 3 above, the product is not necessarily $Zn(OH)_4^{2-}$, nevertheless, other forms may be produced such as $Zn(OH)^+$, $Zn(OH)_2$, or $Zn(OH)_3^-$,

depending on the concentration of Zn^{2+} and OH^- ions [49].

When ZnO NPs are prepared without using a protective agent such as starch, it is found that most of the NPs existed in agglomerated form as confirmed by DLS characterization (see below). ZnO nanoparticles cause an immediate agglomeration during synthesis due to the Vander wall forces of attraction [47]. When the concentration of Zn^{2+} ions or OH^- ions increases without starch, supersaturated ZnO nuclei would more freely agglomerate, and so larger ZnO particles would growing [42]. The mechanism of stabilization by starch could be either due to its capability to increase the viscosity of the solution, or its ability to produce complexes with metallic ions through its hydroxyl groups of the particular D-glucose monomers [50]. Moreover, the soluble starch protects and prevents the ZnO NPs from agglomeration by the action of steric or electrostatic hindrance and so stabilizing the ZnO NPs [47].

The role of starch in the stabilization of ZnO NPs was schematically suggested and presented in Fig. 7. Among the various organic ligands employed as protective agents, starch has a high chemical reactivity in comparison to other saccharides, due to the high reactivity of the OH groups of its α-glucose units [27]. The lone pairs of electrons at their oxygen atoms are capable of playing the role of ligands for coordinating to zinc ions to form a zinc-starch complex (Fig. 7 (First step)) and thus may provide the stability to ZnO NPs formed. When the solution of NaOH is added, the zinc-starch complex reacts with OH^- ions to form $Zn(OH)_4^{2-}$ around the OH groups of starch (Fig. 7 (Second step)). Then, $Zn(OH)_4^{2-}$ dehydrates by drying and calcination into ZnO near the starch; the adsorption of starch onto ZnO NPs surface as suggested in Fig. 7 (Third step) indicates that starch serves as an obstructer of aggregation and acts as a good stabilizer of ZnO NPs.

Moreover, the ZnO particle growth, flocculation, and coagulation can be governed well by the nanonetworks created by the molecules of starch in solution. Hence, ZnO NPs could not move easily, and they were uniformly dispersed in the nanonetwork [51]. Meanwhile, with using starch as a stabilizer, the concentration of unbonded Zn^{2+} ions is immensely decreased as a result of the combination of the OH groups of starch and Zn^{2+} ions [42] and so the movability of Zn^{2+} ions and the growth of the ZnO NPs are well-controlled [27]. Stabilizing of starch for ZnO NPs was also supported by IR data (see below) which indicated the interaction of starch with ZnO NPs. Also, the small nano-size of ZnO NPs obtained using starch as a stabilizer was confirmed with DLS and TEM characterizations (See below).

3.3. Characterization of tuned ZnO NPs

From the discussion above, it is concluded that the optimized ZnO NPs sample was obtained using starch as a stabilizer at reaction conditions of 0.5 h, room temperature (25 °C), 1:2 (M_{Zn}:M_{NaOH}) ratio and 1% (w/v) starch concentration. That sample was then characterized by FT-IR, DLS, ζ-P, and TEM.

3.3.1. FT-IR spectrum

To further support the formation and stabilization mechanism of ZnO NPs, FT-IR studies were performed and the FT-IR spectra of the synthesized ZnO NPs, acquired in the 4000-400 cm^{-1} wavenumber range, were shown in Fig. 8.

The assignments of the main peaks are listed in Table 4 [26, 27, 52-55] according to the FT-IR spectra obtained. FT-IR spectra (Fig. 8) confirmed the presence of specific bands corresponding to several functional groups indicated that starch successfully acts as a capping agent for ZnO NPs. Functional groups on the surface of ZnO NPs can make these particles suitable for antibacterial and biomedical applications [13].

The spectrum shows the characteristic bands indicating saccharide structure with glucopyranose rings of starch used as a capping agent, such as O—H stretching broad band at 3290.20 cm^{-1}, C—H stretching at 2930.11 cm^{-1}, C—O—C stretching at 1148.05 cm^{-1}, C—O stretching at 1076.50 cm^{-1}. Wave number value at 3290 cm^{-1} is characteristic of intermolecular bonded O—H, which probably due to the interaction between ZnO NPs and hydroxyl groups of starch as a capping agent. Also, the characteristic C—O—C ring vibration on starch cause absorbance bands at around 859.33 cm^{-1} and 762.11 cm^{-1}. The C—O bending associated with the O-H group would leads to an absorbance peak at around 1635.41 cm^{-1}. The peak at 1336.55 cm^{-1} is assigned to the O—H bending. The standard peaks correspond to Zn—O stretching vibrations appears at 573.43 cm^{-1}, 522.51 cm^{-1}, and 438.15 cm^{-1} that confirm the successful production of ZnO NPs. This result of Zn—O stretching is consistent with a previous work cited by Darvishi et al. [13] for the synthesis of ZnO NPs by chemical and green methods that reported the presence of a peak at 439 cm^{-1}. Four ZnO/cellulose samples were synthesized by Li et al. [56] showed the appearance of Zn—O stretching bands at 426.4 cm^{-1} and 557.6 cm^{-1} that confirmed the existence of ZnO nanocrystals. Previously, it has been recorded that the bands

between 450 and 800 cm^{-1} were attributed to the vibration of the Zn—O bond [57].

.

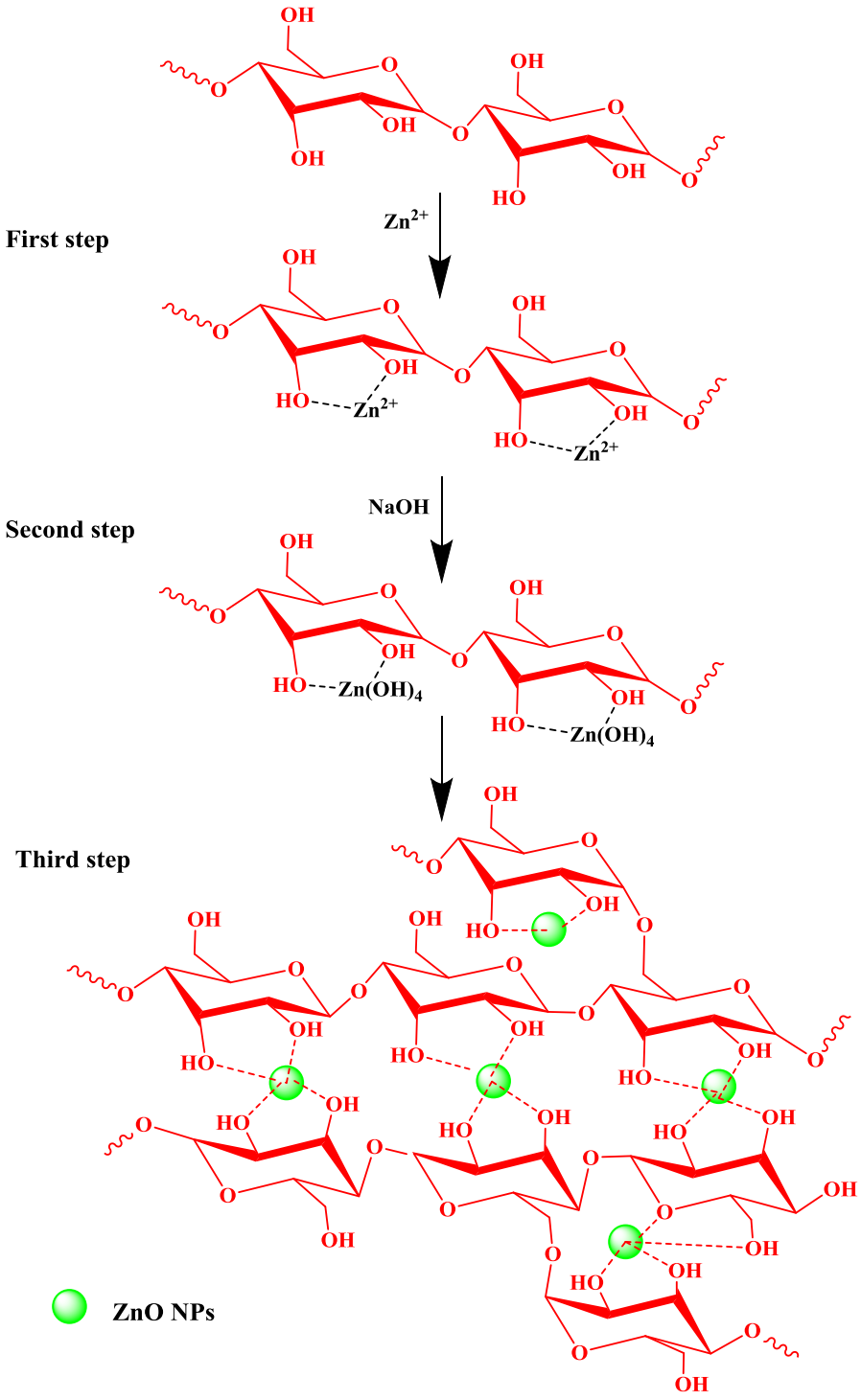

Fig. 7. Schematic representation of starch's role in the stabilization of ZnO NPs.

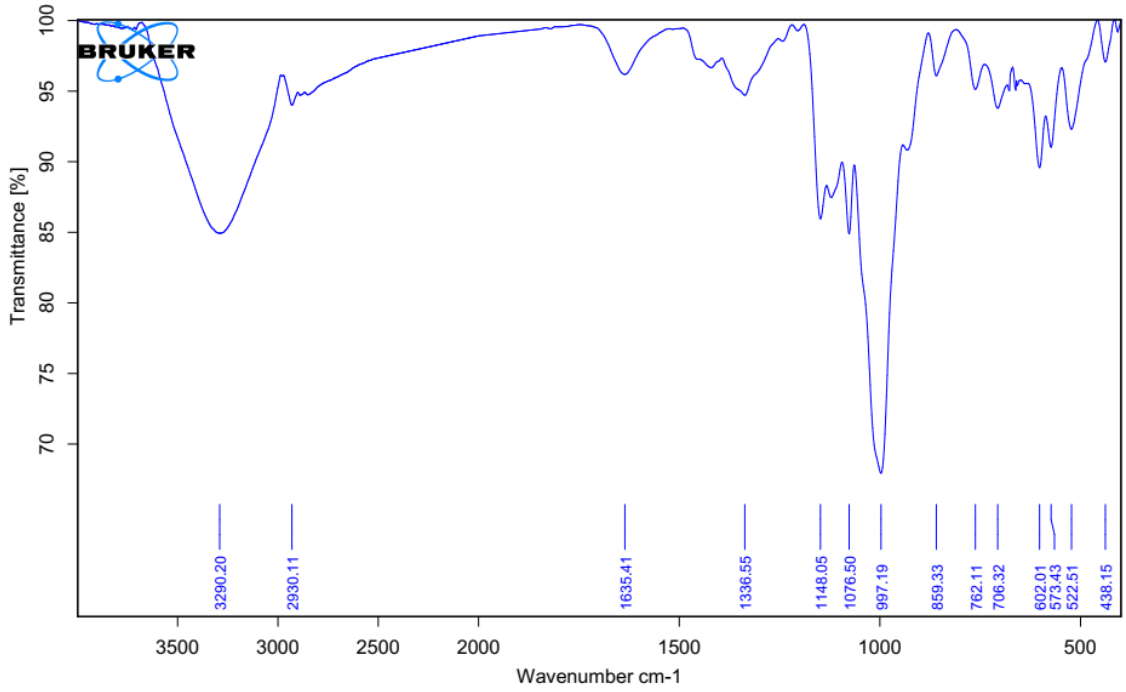

Fig. 8. FT-IR spectra of starch stabilized ZnO NPs.

Table 4. Signal assignments for FT-IR spectra of ZnO NPs stabilized by starch.

Wave number (cm^{-1})	Band assignment
3290.20	O—H stretching (intermolecular bonded)
2930.11	C—H stretching
1635.41	C—O bending associated with O-H group or absorbed water
1336.55	O—H (in-plane) bending
1148.05	C—O—C asymmetric stretching
1076.50, 997.19	C—O stretching
859.33, 762.11	C—O—C ring vibration of carbohydrate
706.32, 602.01	O—H (out-of-plane) bending or Zn—O stretching
573.43, 522.51, 438.15	Zn—O stretching

3.3.2. DLS for particle size analysis

DLS is a popularly used and emerging technique for the determination of particle size in a colloidal solution based on Brownian movement. The size of NPs is one of the most critical characteristics for the application of nanoparticles in many fields, especially in the biomedical field. The DLS histograms of ZnO NPs prepared without stabilizer and using starch, CMC, and HEC stabilizers, respectively, are depicted in Fig. 9a-d. As is seen in Fig. 9a, without using a stabilizer, the average size of ZnO particles was 282.6 nm. On the opposite hand, in the presence of a stabilizer, as observed in Fig. 9b-d for particle size analysis, it has absolutely proved that the synthesized ZnO NPs were distributed in nanosize form (less than 100 nm); the average sizes of ZnO NPs obtained using starch, CMC and HEC stabilizers were 68.43 nm, 71.47 nm, and 86.08 nm, respectively. The smaller nano-sizes exhibited by ZnO NPs obtained using the three stabilizers studied make them good candidates for biomedical applications.

The DLS results (Fig. 9) are indeed in the agreement with the results obtained by UV-Vis analysis for the preparation of ZnO NPs using starch, CMC, and HEC stabilizers at 0.5 h (Fig. 3) and without using a stabilizer (0%) (Fig. 6). As illustrated earlier, ZnO NPs tend to agglomerate easily during chemical precipitation without a stabilizer due to the Vander wall forces of attraction result from their high surface energies and their large surface areas [47]. On the other hand, in the presence of a stabilizer, a surface coating surrounding the particles is formed, which reduces the interaction between the

nanoparticles and prevents it from agglomeration. As reported from both UV-Vis data and DLS results of this investigation, the smallest average size (68.43 nm) was related to ZnO NPs stabilized by starch. The important role of starch as a stabilizer was suggested previously (Fig. 7) which indicated the interaction of starch through its hydroxyl groups with ZnO NPs. The differences in the average sizes of ZnO NPs stabilized by starch, CMC, and HEC may be attributed to differences in stabilizers structures reported in Fig. 1 that may lead to differences in binding abilities between Zn^{2+} ions and the hydroxyl oxygens of starch, CMC, and HEC, resulting in different stabilizing effects.

The UV-Vis spectra and DLS results also indicated that ZnO NPs obtained using cellulose derivatives (CMC and HEC) were bigger than that of starch stabilized nanoparticles. The β-1,4 linkage between the glucose monomers in cellulose derivatives (Fig. 1) results in the polymeric chain being very straight. As a result, CMC and HEC molecules can pack together closely (imagine a bunch of straight, parallel rods) and that permits a great deal of intermolecular hydrogen bonding between the adjacent chains. In contrast, the α-1,4 linkage in starch (Fig. 1) produces a loose helical structure that keeps the molecules from being able to maintain large amounts of side-by-side contact. So, the crystalline capacity of starch is lower than that of cellulose derivatives. Hence, Zn^{2+} ions more readily bind with the hydroxyl oxygens of the molecular chain of starch, which decreases the intermolecular H-bonding, and reduces the crystalline regions of starch [51]. Therefore, the nanoparticles prepared with starch as a stabilizer were the smallest.

3.3.3. Measurement of zeta potential

Zeta potential (ζ-P) is a measure of the potential difference between the mobile dispersion medium in which a particle is dispersed and the stationary layer of the dispersion medium containing the counter-charged ions attached to the dispersed nanoparticles [58, 59]. ζ-P determination is a significant characterization technique to estimate the surface charge of nanoparticles, which is useful in the determination of the colloidal stability of NPs [59]. Hence, the surface charge of ZnO NPs was determined by ζ-P analysis and given in Fig. 10. ZnO NPs showed a mean ζ-P of −21.6 mV, explaining that they are moderately stable.

A high positive or negative value of ζ-P demonstrates better physical NPs stability due to electrostatic repulsions between the single charged NPs in the dispersion. On the other hand, particles with low ζ-P tend to coagulate or flocculate due to the Van der Waals attractive forces act upon them, presumably causing poor physical stability [60]. In general, when the ζ-P of nanosuspension is large, the repulsive forces highly exceed the attractive forces, results in a somewhat stable system.

A similar value (−20.9 mV) of ζ-P is obtained for ZnO NPs synthesized using the leaf extract of *Cinnamomum tamala* [61]. Nithya and Kalyanasundharam [62] reported the ζ-P of ZnO NPs in the range of −32.06 to −17.89 mV that indicated that the stability of the ZnO NPs is moderate. In our study, the coating of the surface of ZnO NPs using starch might be a possible reason for their moderate stability that makes them a plausible candidate for antibacterial activity application.

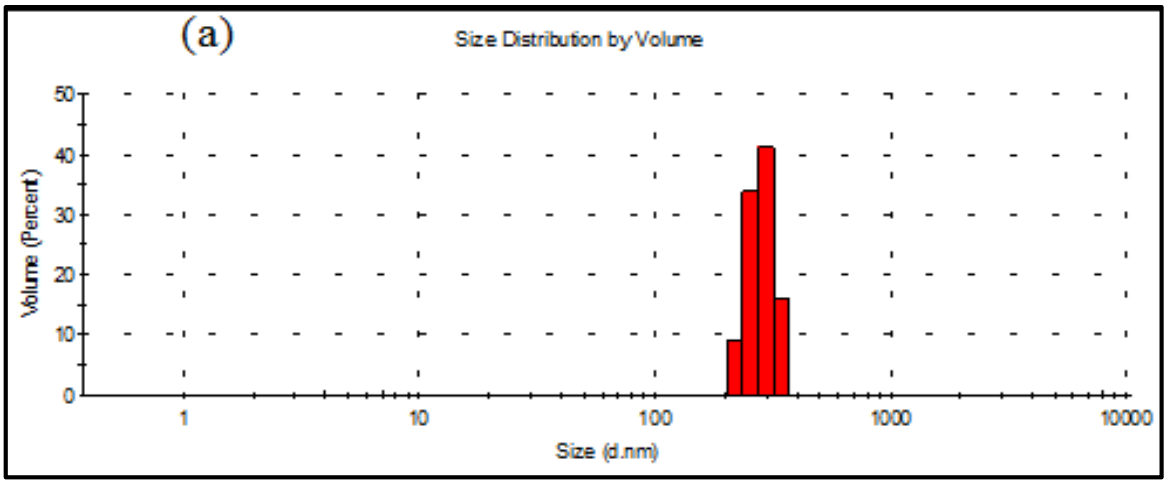

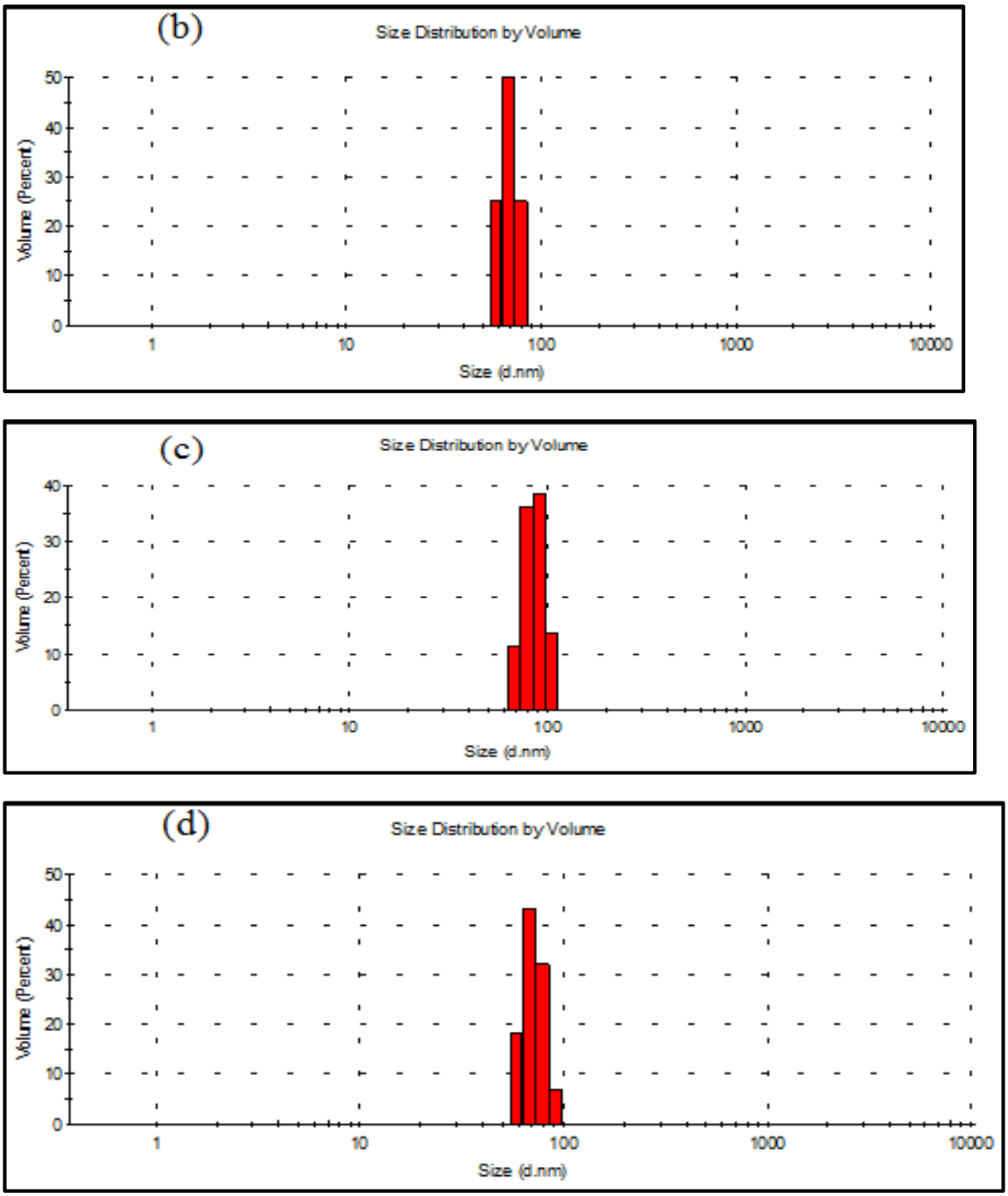

Fig. 9. DLS histograms of ZnO NPs prepared (a) without using stabilizer (time: 0.5 h; temperature: 25 °C; M_{Zn}:M_{NaOH} = 1:2) and using (b) starch, (c) CMC and (d) HEC stabilizers (time: 0.5 h; temperature: 25 °C; M_{Zn}:M_{NaOH} = 1:2, stabilizer concentration: 1%).

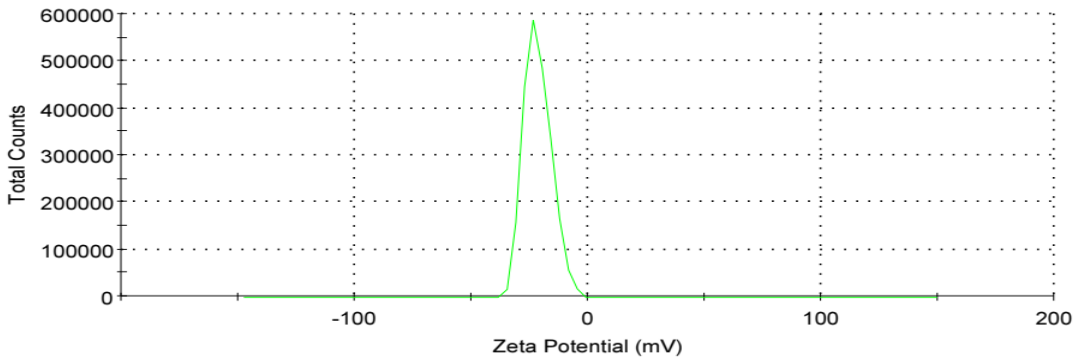

Fig. 10. Zeta potential analysis of starch stabilized ZnO NPs.

3.3.4. TEM analysis

The morphology of ZnO NPs synthesized using 1% starch as a stabilizer was examined using TEM and a typical micrograph is shown in Fig. 11.

The micrograph reveals that the particles are not completely dispersed and there are some aggregates, due to the large surface energy established by ZnO NPs that results in an agglomeration, particularly when synthesis is performed in an aqueous solution. As indicated from Fig. 11, the ZnO NPs are almost spherical with an average size of 23 nm which was determined using ImageJ software. Vigneshwaran et al. [63] synthesized ZnO-soluble starch nanocomposites in the presence of 0.5% starch as a stabilizer. In their study, TEM images showed numerous ZnO NPs embedded into soluble starch granules with varying sizes from 50 to 2000 nm. Besides, there was an aggregation in the NPs, which was probably induced by the presence of starch [63, 64].

It is found in our study that the average particle size measured by TEM (23 nm) is lower than the one reported by DLS (68.43 nm). This difference between TEM and DLS is consistent with many previous investigations reported on the synthesis of various NPs [65-67]. The principal differences between the diameters determined from DLS and TEM techniques are probable due to the existence of an adsorbing layer of coating agent [66, 67]; DLS analysis has a high sensitivity to the adsorbed layer of starch onto the surface of the ZnO NPs. The large difference noted for the size measured by DLS and TEM in small-sized NPs, is principally attributed to the radius of curvature effect [66, 67].

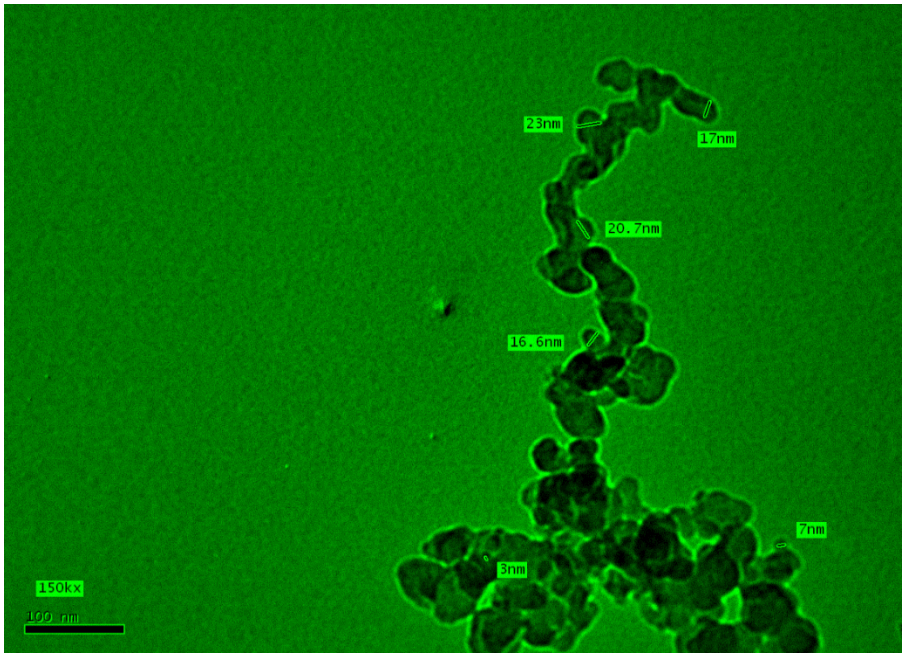

Fig. 11. TEM micrograph of starch stabilized ZnO NPs.

3.4. Evaluation of the antibacterial activity of ZnO NPs

Among the different metal oxides NPs, ZnO NPs have been found to have strong antibacterial activities [1, 68] due to their unique characteristics [7]. Moreover, ZnO NPs are adequate for antimicrobial applications because of their stability under severe processing conditions [69, 70]. Different techniques are used to evaluate antibacterial activity in vitro. The most common one is through the agar well diffusion technique due to its simplicity and cost-effectiveness [29, 68].

Antibacterial activity of ZnO NPs was evaluated based on the zone of inhibition (ZOI) against two Gram-positive bacteria (*B. subtilis* and *S. epidermidis*) and two Gram-negative bacteria (*E. cloacae* and *E. coli*) (Fig. 12). The clear ZOI created around the wells were detected and expressed in mm (Table 5).

The current study obviously indicated a strong antibacterial activity of ZnO NPs against *B. subtilis*, *S. epidermidis*, and *E. cloacae* and it showed moderate activity against *E. coli*. From the results in Table 5, it was observed that the highest ZOI for Gram-positive bacteria was 17 mm in *B. subtilis* and the lowest ZOI was 14 mm in *S. epidermidis*. For Gram-negative bacteria, the highest ZOI was 16 mm in *E. cloacae* whereas *E. coli* showed the lowest ZOI at 10 mm. The highest inhibitory action of ZnO NPs was manifested against *B. subtilis* followed by *E. cloacae*, *S. epidermidis*, and *E. coli*. Besides, ZnO NPs showed a higher antibacterial effect against Gram-positive than the Gram-negative bacteria with the exception of the lower activity noted for *S. epidermidis* (14 mm) as compared to that of *E. cloacae* (16 mm) (Table 5).

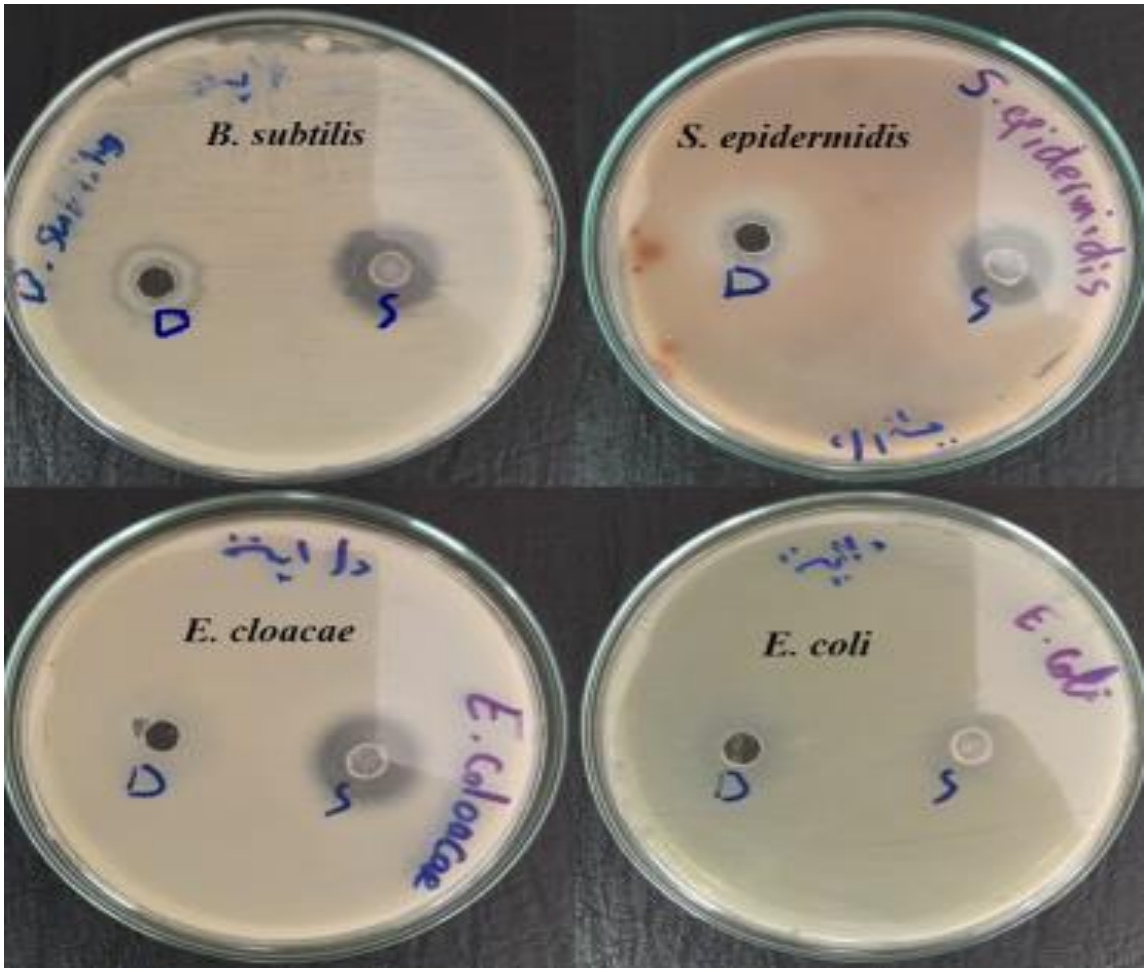

Fig. 12. Antibacterial activity of starch stabilized ZnO NPs (D: DMSO, S: ZnO NPS).

Table 5. Mean zone of inhibition (ZOI) of ZnO NPs against different pathogenic microorganisms.

Tested microorganisms	ZOI (mm)[a]	
	ZnO NPs	Positive control[b]
Gram-positive bacteria		
B. subtilis	17 ± 0.12	26 ± 0.21
S. epidermidis	14 ± 0.15	28 ± 0.24
Gram-negative bacteria		
E. cloacae	16 ± 0.17	30 ± 0.27
E. coli	10 ± 0.09	30 ± 0.30

[a] Results are expressed as the mean of three separate trials ± Standard Deviation.

[b] Reference drugs: Ciprofloxacin for Gram-positive and Gentamicin for Gram-negative strains.

Earlier research reports also demonstrated that the antibacterial activity of ZnO NPs was greater on Gram-positive than Gram-negative bacteria [68]. El Saeed et al. [71] tested the antibacterial activity of ZnO polyurethane nanocomposite against Gram-negative (*E. coli*) and Gram-positive (*B. subtilis*). It was noted that Gram-positive was more affected than Gram-negative bacteria. Elmi et al. [72] investigated the antibacterial activity of ZnO NPs against *K. pneumoniae*, *E. coli*, *Proteus*, and *S. epidermidis* bacteria in wastewater. Based on their results, ZnO NPs had the most effect against Gram-positive bacteria *S. epidermidis*.

The reasons for sensitivity differences between Gram-positive and Gram-negative bacteria might be mainly attributed to differences in their cell wall structure [73]. The cell walls of Gram-positive bacteria composed mostly of peptidoglycan. The peptidoglycan layer consists of networks with lots of pores, which is not an effective permeability barrier. In contrast, cell walls of Gram-negative bacteria consist of only a thin layer of peptidoglycan and an outer membrane composed of phospholipids, lipopolysaccharide, and lipoprotein. The complicated bilayer cell structure of Gram-negative bacteria causes the outer membrane to acts as a potential barrier against foreign molecules and makes the cell wall to be less permeable to antibacterial agents.

On the contrary, the lower ZOI noted for Gram-positive *S. epidermidis* (14 mm) as compared to that of Gram-negative *E. cloacae* (16 mm) may be due to the thick layer of peptidoglycan (20-80 nm) in the cell wall of Gram-positive bacteria that may act as an additional barrier for the entry of nanoparticles inside the cells [74, 75]. On the other hand, Gram-negative bacteria cell wall is thinner (8-10 nm) that facilitates passive diffusion of ZnO NPs inside the cell [74, 76, 77]. The degeneration of the cell wall by the nanoparticle attachment is a first mechanism of the antimicrobial action [78]; actually, the predominant mechanism by which ZnO NPs actively suppress the bacterial growth is the main reason for the sensitivity difference between Gram-positive and Gram-negative bacteria.

The high resistance of Gram-positive *S. epidermidis* cells towards the nanotoxic effect of ZnO NPs than Gram-negative *E. cloacae* in this investigation agrees with some results reported in the literature [75, 78]. Zare et al. [75] estimated the antimicrobial activities of ZnO NPs using the disk diffusion technique in different strains of bacteria, which showed that the sensitivity of Gram-negative bacteria was more than that of Gram-positive bacteria. Al-Kordy et al. [78] also revealed that the antibacterial activity of *Alkalibacillus* sp.w7 synthesized ZnO NPs were more efficient against Gram-negative compared to Gram-positive bacterial pathogens.

3.4.1. Antibacterial mechanism of ZnO NPs

Some possible antibacterial mechanisms were proposed in the literature to understand the antibacterial activity of ZnO NPs [37, 68, 79-83]. These can be summarized as follows (Fig. 13):

1. Release of Zn^{2+} ions: in this mechanism, ZnO NPs gradually release Zn^{2+} ions that can permeate the cell membrane and leads to the denaturation of protein and the termination of cell proliferation. Moreover, Zn^{2+} can also damage the electron transport system, causing a cellular respiratory disorder [80]. Many bacterial cell actions such as enzyme activity and bacterial metabolism, etc., are inhibited by the action of released toxic Zn^{2+} ions from ZnO NPs, causing bacterial cell death [84].

2. Generation of Reactive Oxygen Species (ROS): the ROS generated from the surface of ZnO NPs is one of the most significant and widely recognized mechanism for the inhibition of bacterial growth adopted by ZnO NPs [83, 85]. Examples of ROS generated are superoxide anion (O_2^-), hydroxyl radical ($^{\bullet}OH$), peroxide anion (O_2^{2-}), hydroxyl anion (OH^-), and hydrogen peroxide (H_2O_2) species that cause lethal damage to bacteria [68, 83]. The damage of DNA, cell membranes, and cellular proteins is

noted through the oxidative stress caused by ROS [68]. The ROS generated also destroy the active components that are responsible for keeping the normal physiological and morphological roles of the microorganism, leads to cell death [86].

3. Direct interaction of ZnO NPs with cell membrane: another possible mechanism is through the direct interaction between the bacterial cell membrane and ZnO NPs via electrostatic forces which leads to changes in microenvironment into the contact areas of the bacterial cell and NPs [68, 87]. This contact may alter the membrane structure resulting in the leaking of intracellular contents that ends with cell death [88]. Brayner et al. [89] also indicated that cell walls were damaged after interaction with ZnO NPs. Moreover, membrane permeability is increased leading to subsequent cellular internalization of ZnO NPs.

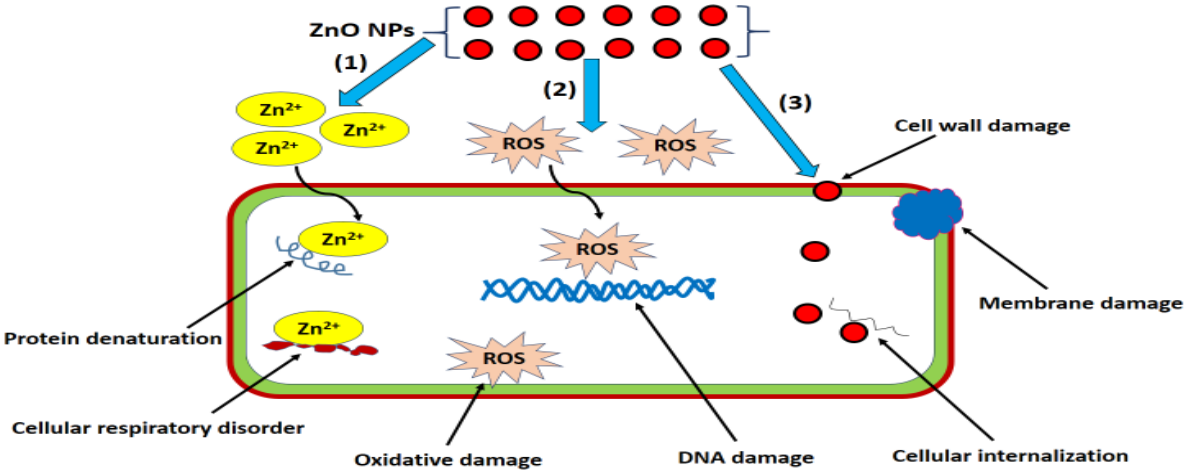

Fig. 13. Schematic representation of ZnO NPs antibacterial mechanisms.

3.4.2. Comparison with other bacteriostatic agents

The antibacterial activities of ZnO NPs prepared in this work and other ZnO NPs in the literature against the four bacteria tested (*B. subtilis*, *S. epidermidis*, *E. cloacae*, and *E. coli*) using the agar diffusion method were compared based on their corresponding ZOI values and were summarized in Table 6. It is illustrated that the ZOI values of ZnO NPs in this work are comparable to or even larger than those reported in the literature. It should be noted that these ZOI values are calculated under their respective experimental conditions. Different methodologies (e.g., technique, time, NPs size, concentration, etc.) reflect the contradictory results in the literature [97]. In general, ZnO NPs synthesized exhibited comparatively remarkable antibacterial activity against tested bacteria.

Table 6. Comparison of ZOI (mm) values between ZnO NPs in this work with other ZnO NPs in the literature.

B. subtilis	*S. epidermidis*	*E. cloacae*	*E. coli*	References
17	14	16	10	This work
			5.7	[90]
			9.5	[91]
	7.67			[92]
14		13		[78]
15				[93]
	15		12.5	[94]
16			15	[79]
	18		12	[72]
		17		[95]
18				[75]
19			12	[20]
		19		[96]

4. Conclusion

Environmentally friendly biopolymers of polysaccharides such as starch, carboxymethyl cellulose (CMC), and hydroxyethyl cellulose (HEC) are successfully introduced as alternative greener and safer materials to the current chemical stabilizers used in the synthesis of zinc oxide nanoparticles (ZnO NPs). The optimum ZnO NPs samples at various synthesis conditions were determined based on their UV-Vis absorption peaks and confirmed using DLS analysis for particle size. It is concluded that the optimized ZnO NPs sample was obtained using starch as the optimum stabilizer at reaction conditions of 0.5 h, room temperature (25 °C), 1:2 (M_{Zn}:M_{NaOH}) ratio and 1% (w/v) starch concentration. It is found that the particle size increased with increasing temperature and NaOH molar concentration that agreed with previous reports in the literature. FT-IR spectra confirmed the presence of specific bands corresponding to several functional groups indicated that starch successfully acts as a capping agent for ZnO NPs. The mechanism of the role of starch in the stabilization of ZnO NPs was suggested. The standard peaks correspond to Zn—O stretching vibrations appears at 573.43 cm^{-1}, 522.51 cm^{-1}, and 438.15 cm^{-1} that confirm the successful formation of ZnO NPs. ZnO NPs showed a mean zeta potential (ζ-P) of −21.6 mV, explaining that they are moderately stable. As indicated from TEM analysis, the ZnO NPs are almost spherical with an average size of 23 nm. The antibacterial assay indicated a strong antibacterial activity of ZnO NPs against *B. subtilis*, *S. epidermidis*, and *E. cloacae* and it showed moderate activity against *E. coli*. The zone of inhibition (ZOI) values of ZnO NPs in this study are comparable to or even larger than those reported in the literature. The synthesis of ZnO NPs by this approach is simple, rapid, green, and cost-effective. Therefore, synthesized ZnO NPs are expected to be a good candidate for antibacterial activity, bio-remediation, drug delivery, catalysis, and other biomedical applications.

Conflicts of interest

"There are no conflicts to declare".

References

1. S. Zhao, C. Guo, Y. Hu, Y. Guo, Q. Pan, The preparation and antibacterial activity of cellulose/ZnO composite: a review, Open Chem. 16 (2018) 9-20, https://doi.org/10.1515/chem-2018-0006.
2. M. Abu-Elghait, M. Hasanin, A.H. Hashem, S.S. Salem, Ecofriendly novel synthesis of tertiary composite based on cellulose and myco-synthesized selenium nanoparticles: Characterization, antibiofilm and biocompatibility, Int. J. Biol. Macromol. 175 (2021) 294–303, https://doi.org/10.1016/j.ijbiomac.2021.02.040.
3. S. Dacrory, A.H. Hashem, M. Hasanin, Synthesis of cellulose based amino acid functionalized nano-biocomplex: Characterization, antifungal activity, molecular docking and hemocompatibility, Environ. Nanotechnol. Monit. Manag. 15 (2021) 100453, https://doi.org/10.1016/j.enmm.2021.100453.
4. M. Hasanin, A. El-Henawy, W.H. Eisa, H. El-Saied, M. Sameeh, Nano-amino acid cellulose derivatives: Eco-synthesis, characterization, and antimicrobial properties, Int. J. Biol. Macromol. 132 (2019) 963–969, https://doi.org/10.1016/j.ijbiomac.2019.04.024.
5. T. Naseem, T. Durrani, The role of some important metal oxide nanoparticles for wastewater and antibacterial applications: A review, Environ. Chem. Ecotoxicol. 3 (2021) 59-75, http://dx.doi.org/10.1016/j.enceco.2020.12.001.
6. J.W. Rasmussen, E. Martinez, P. Louka, D.G. Wingett, Zinc oxide nanoparticles for selective destruction of tumor cells and potential for drug delivery applications, Expert Opin. Drug Deliv. 7 (2010) 1063–1077, https://doi.org/10.1517/17425247.2010.502560.
7. A.R. Prasad, L. Williams, J. Garvasis, K.O. Shamsheera, S.M. Basheer, M. Kuruvilla, A. Joseph, Applications of phytogenic ZnO nanoparticles: A review on recent advancements, J. Mol. Liq. 331 (2021) 115805, https://doi.org/10.1016/j.molliq.2021.115805.
8. D.D. La, P. Nguyen-Tri, K.H. Le, P.T.M. Nguyen, M.D. Nguyen, A.T.K. Vo, M.T.H. Nguyen, S.W. Chang, L.D. Tran, W.J. Chung, D.D. Nguyen, Effects of antibacterial ZnO nanoparticles on the performance of a chitosan/gum arabic edible coating for post-harvest banana preservation, Prog. Org. Coat. 151 (2021) 106057, https://doi.org/10.1016/j.porgcoat.2020.106057.
9. C. Pokhum, V. Intasanta, W. Yaipimai, N. Subjalearndee, C. Srisitthiratkul, V. Pongsorrarith, N. Phanomkate, C. Chawengkijwanich, A facile and cost-effective method for removal of indoor airborne psychrotrophic bacterial and fungal flora based on silver and zinc oxide nanoparticles decorated on fibrous air filter, Atmos. Pollut. Res. 9 (2018) 172-177, http://dx.doi.org/10.1016/j.apr.2017.08.005.

10. M. Ahmad, W. Rehman, M.M. Khan, M.T. Qureshi, A. Gul, S. Haq, R. Ullah, A. Rab, F. Menaa, Phytogenic fabrication of ZnO and gold decorated ZnO nanoparticles for photocatalytic degradation of Rhodamine B, J. Environ. Chem. Eng. 9 (2021) 104725, https://doi.org/10.1016/j.jece.2020.104725.
11. J. Jiang, J. Pi, J. Cai, The advancing of zinc oxide nanoparticles for biomedical applications, Bioinorg. Chem. Appl. 2018 (2018), https://doi.org/10.1155/2018/1062562.
12. V. Tiwari, N. Mishra, K. Gadani, P.S. Solanki, N.A. Shah, M. Tiwari, Mechanism of anti-bacterial activity of zinc oxide nanoparticle against carbapenem-resistant acinetobacter baumannii, Front. Microbiol. 9 (2018) 1218, https://doi.org/10.3389/fmicb.2018.01218.
13. E. Darvishi, D. Kahrizi, E. Arkan, Comparison of different properties of zinc oxide nanoparticles synthesized by the green (using Juglans regia L. leaf extract) and chemical methods, J. Mol. Liq. 286 (2019) 110831, https://doi.org/10.1016/j.molliq.2019.04.108.
14. A. Katiyar, N. Kumar, R.K. Shukla, A. Srivastava, Influence of alkali hydroxides on synthesis, physico-chemical and photoluminescence properties of zinc oxide nanoparticles, Mater. Today Proc. 29 (2020) 885–889, https://doi.org/10.1016/j.matpr.2020.05.112.
15. H. Dhasmana, V. Dutta, A. Kumar, A. Kumar, A. Verma, V.K. Jain, Hydrothermally synthesized zinc oxide nanoparticles for reflectance study onto Si surface, Mater. Today Proc. 32 (2020) 287–293, https://doi.org/10.1016/j.matpr.2020.01.374.
16. I. Kim, K. Viswanathan, G. Kasi, K. Sadeghi, S. Thanakkasaranee, J. Seo, Preparation and characterization of positively surface charged zinc oxide nanoparticles against bacterial pathogens, Microbial Pathogenesis 149 (2020) 104290, https://doi.org/10.1016/j.micpath.2020.104290.
17. A. Kumar, Sol gel synthesis of zinc oxide nanoparticles and their application as nano-composite electrode material for supercapacitor, J. Mol. Struct. 1220 (2020) 128654, https://doi.org/10.1016/j.molstruc.2020.128654.
18. J. Ding, S. Chen, N. Han, Y. Shi, P. Hu, H. Li, J. Wang, Aerosol assisted chemical vapour deposition of nanostructured ZnO thin films for NO_2 and ethanol monitoring, Ceram. Int. 46 (2020) 15152–15158, https://doi.org/10.1016/j.ceramint.2020.03.051.
19. R. Suntako, Effect of zinc oxide nanoparticles synthesized by a precipitation method on mechanical and morphological properties of the CR foam, Bull. Mater. Sci. 38 (2015) 1033–1038, https://doi.org/10.1007/s12034-015-0921-0.
20. J.E. Jeronsia, L.A. Joseph, S.J. Das, Investigations on anticancer and antibacterial activities of zinc oxide nanoparticles, Int. J. Dev. Res. 5 (2015) 5707-5711.
21. E. Darezereshki, M. Alizadeh, F. Bakhtiari, M. Schaffie, M. Ranjbar, A novel thermal decomposition method for the synthesis of ZnO nanoparticles from low concentration $ZnSO_4$ solutions, Appl. Clay Sci. 54 (2011) 107–111, https://doi:10.1016/j.clay.2011.07.023.
22. S.R. Brintha, M. Ajitha, Synthesis and characterization of ZnO nanoparticles via aqueous solution, sol-gel and hydrothermal methods, IOSR-JAC 8 (2015) 66-72, https://doi:10.9790/5736-081116672.
23. M. Mohammadian, Z. Es'haghi, S. Hooshmand, Green and chemical synthesis of zinc oxide nanoparticles and size evaluation by UV–vis spectroscopy, J. Nanomed. Res. 7 (2018) 00175, https://doi:10.15406/jnmr.2018.07.00175.
24. H. Duan, D. Wang, Y. Li, Green chemistry for nanoparticle synthesis, Chem. Soc. Rev. 44 (2015) 5778–5792, https://doi.org/10.1039/C4CS00363B.
25. S. Kango, S. Kalia, A. Celli, J. Njuguna, Y. Habibi, R. Kumar, Surface modification of inorganic nanoparticles for development of organic–inorganic nanocomposites-A review, Prog. Polym. Sci. 38 (2013) 1232–1261, http://dx.doi.org/10.1016/j.progpolymsci.2013.02.003.
26. A. Shehabeldine, M. Hasanin, Green synthesis of hydrolyzed starch–chitosan nano-composite as drug delivery system to gram negative bacteria, Environ. Nanotechnol. Monit. Manag. 12 (2019) 100252, https://doi.org/10.1016/j.enmm.2019.100252.
27. A.K. Zak, W.H.A. Majid, M.R. Mahmoudian, M. Darroudi, R. Yousefi, Starch-stabilized synthesis of ZnO nanopowders at low temperature and optical properties study, Adv. Powder Technol. 24 (2013) 618–624, http://dx.doi.org/10.1016/j.apt.2012.11.008.
28. S. Azizi, M. Ahmad, M. Mahdavi, S. Abdolmohammadi, Preparation, characterization, and antimicrobial activities of ZnO nanoparticles/cellulose nanocrystal nanocomposites, Bioresources 8 (2013) 1841-

1851, https://doi.org/10.15376/biores.8.2.1841-1851.
29. C. Perez, M. Paul, P. Bazerque, Antibiotic assay by agar-well diffusion method, Acta Biol. Med. Exp. 15 (1990) 113-115.
30. M.M. AbdElhady, Preparation and characterization of chitosan/zinc oxide nanoparticles for imparting antimicrobial and UV protection to cotton fabric, Int. J. Carbohydr. Chem. (2012), https://doi.org/10.1155/2012/840591.
31. M. Darroudi, M.B. Ahmad, R. Zamiri, A. Zak, A. Abdullah, N.A. Ibrahim, Time-dependent effect in green synthesis of silver nanoparticles, Int. J. Nanomedicine 6 (2011) 677-681, https://doi.org/10.2147/IJN.S17669.
32. I. Venditti, T.F. Hassanein, I. Fratoddi, L. Fontana, C. Battocchio, F. Rinaldik, M. Carafa, C. Marianecci, M. Diociaiuti, E. Agostinelli, C. Cametti, M.V. Russo, Bioconjugation of gold-polymer core-shell nanoparticles with bovine serum amine oxidase for biomedical applications, Colloids Surf. B 134 (2015) 314-321, http://dx.doi.org/10.1016/j.colsurfb.2015.06.052.
33. M.B. Ahmad, J.J. Lim, K. Shameli, N.A. Ibrahim, M.Y. Tay, B.W. Chieng, Antibacterial activity of silver bionanocomposites synthesized by chemical reduction route, Chem. Cent. J. 6 (2012) 1–9, https://doi.org/ 10.1186/1752-153X-6-101.
34. S.K. Balavandy, K. Shameli, D.R.B.A. Biak, Z.Z. Abidin, Stirring time effect of silver nanoparticles prepared in glutathione mediated by green method, Chem. Cent. J. 8 (2014) 1–10, https://doi.org/ 10.1186/1752-153X-8-11.
35. S.L. Smitha, K.M. Nissamudeen, D. Philip, K.G. Gopchandran, Studies on surface plasmon resonance and photoluminescence of silver nanoparticles, Spectrochim. Acta A Mol. Biomol. Spectrosc. 71 (2008) 186-190, https://doi.org/10.1016/j.saa.2007.12.002.
36. Z.R. Dai, Z.W. Pan, Z.L. Wang, Novel nanostructures of functional oxides synthesized by thermal evaporation, Adv. Funct. Mater. 13 (2003) 9-24, https://doi.org/10.1002/adfm.200390013.
37. M. Jyoti, D. Vijay, S. Radha, To study the role of temperature and sodium hydroxide concentration in the synthesis of zinc oxide nanoparticles, IJSRP 3 (2013).
38. B. Baruwati, D.K. Kumar, S.V. Manorama, Hydrothermal synthesis of highly crystalline ZnO nanoparticles: a competitive sensor for LPG and EtOH, Sens. Actuators B Chem. 119 (2006) 676-682, https://doi.org/10.1016/j.snb.2006.01.028.
39. V. Koutu, L. Shastri, M.M. Malik, Effect of NaOH concentration on optical properties of zinc oxide nanoparticles, Mater. Sci. Poland 34 (2016) 819–827, https://doi.org/10.1515/msp-2016-0119.
40. M.R. Nath, A.N. Ahmed, M.A. Gafur, M.Y. Miah, S. Bhattacharjee, ZnO nanoparticles preparation from spent zinc–carbon dry cell batteries: studies on structural, morphological and optical properties, J. Asian Ceram. Soc. 6 (2018) 262- 270, https://doi.org/10.1080/21870764.2018.1507610 .
41. M.A.M. Moazzen, S.M. Borghei, F. Taleshi, Change in the morphology of ZnO nanoparticles upon changing the reactant concentration, Appl. Nanosci. 3 (2013) 295–302, https://doi.org/10.1007/s13204-012-0147-z.
42. Z. Wang, H. Li, F. Tang, J. Ma, X. Zhou, A Facile approach for the preparation of nano-size zinc oxide in water/glycerol with extremely concentrated zinc sources, Nanoscale Res. Lett. 13 (2018) 202, https://doi.org/10.1186/s11671-018-2616-0.
43. P. Chand, A. Gaur, A. Kumar, U.K. Gaur, Effect of NaOH molar concentration on optical and ferroelectric properties of ZnO nanostructures, Appl. Surf. Sci., 356 (2015), 438-446, https://doi.org/10.1016/j.apsusc.2015.08.107.
44. S. Anandhavelu, S. Thambidurai, Effect of zinc chloride and sodium hydroxide concentration on the optical property of chitosan–ZnO nanostructure prepared in chitin deacetylation, Mater. Chem. Phys. 131 (2011) 449-454, https://doi.org/10.1016/j.matchemphys.2011.10.003.
45. W. Ostwald, Lehrbuch der allgemeinen chemie, 2. 1896, Leipzig, Germany.
46. M. Haruta1, B. Delmon, Preparation of homodisperse solids, J. Chim. Phys. 83 (1986) 859 – 868, https://doi.org/10.1051/jcp/1986830859.
47. P. Vasileva, Synthesis and characterization of ZnO nanocrystals in starch matrix, Materials Science. Non-Equilibrium Phase Transformations. 2 (2016), 26-29.
48. S.K. Patra, A novel chemical approach to fabricate ZnO Nanostructure, M.Sc. thesis, Indian Institute of Technology Kharagpur (2008).
49. S. Xu, Z.L. Wang, One-dimensional ZnO nanostructures: solution growth and functional properties, Nano Res. 4 (2011) 1013-1098, https://doi.org/10.1007/s12274-011-0160-7.
50. F. He, D. Zhao, Preparation and characterization of a new class of starch-stabilized bimetallic nanoparticles for degradation of chlorinated hydrocarbons in water, Environ. Sci. Technol. 39

(2005) 3314–3320, https://doi.org/10.1021/es048743y.
51. J. Ma, W. Zhu, Y. Tian, Z. Wang, Preparation of zinc oxide-starch nanocomposite and its application on coating, Nanoscale Res. Lett. 11 (2016) 200, https://doi.org/10.1186/s11671-016-1404-y.
52. A.H.D Abdullah, S. Chalimah, I. Primadona, M.H.G Hanantyo, Physical and chemical properties of corn, cassava, and potato starchs, IOP Conf. Series: Earth and Environmental Science 160 (2018) 012003, https://doi.org/10.1088/1755-1315/160/1/012003.
53. M.G. Lomelí-Ramírez, A.J. Barrios-Guzmán, S. García-Enriquez, J.d.J. Rivera-Prado, R. Manríquez-González, Chemical and mechanical evaluation of bio-composites based on thermoplastic starch and wood particles prepared by thermal compression, Biores. 9 (2014) 2960-2974, https://doi.org/10.15376/biores.9.2.2960-2974.
54. N. Sarifuddin, H. Ismail, Z. Ahmad, Effect of fiber loading on properties of thermoplastic sago starch/kenaf core fiber biocomposites, Biores. 7 (2012) 4294-4306, https://doi.org/10.15376/BIORES.7.3.4294-4306.
55. E. Pretsch, T. Clerc, J. Seibil, W. Simon, Tables of spectral data for structure determination of organic compounds: 13C-NMR, 1H-NMR, IR, MS, UV/VIS Chemical Laboratory Practice. W. Fresenius, J.F.K. Huber, E. Pungor, G.A. Rechnitz, W. Simon, T. S. West (eds.), 2nd edition (1989), Springer-Verlag, Berlin, I5-280.
56. X. Li, L. Zhang, Z. Wang, S. Wu, J. Ma, Cellulose controlled zinc oxide nanoparticles with adjustable morphology and their photocatalytic performances, Carbohydr. Polym. 259 (2021) 117752, https://doi.org/10.1016/j.carbpol.2021.117752.
57. J. Wang, L. Gao, Synthesis and characterization of ZnO nanoparticles assembled in one-dimensional order, Inorg. Chem. Commun. 6 (2003) 877–881, https://doi.org/10.1016/S1387-7003(03)00134-5.
58. V. Selvamani, Chapter 15 - Stability studies on nanomaterials used in drugs, Editor(s): S.S. Mohapatra, S. Ranjan, N. Dasgupta, R. K. Mishra, S. Thomas, In Micro and Nano Technologies, Characterization and biology of nanomaterials for drug delivery, Elsevier (2019) 425-444, https://doi.org/10.1016/B978-0-12-814031-4.00015-5.
59. Z. Abbas, C. Labbez, S. Nordholm, E. Ahlberg, Size-dependent surface charging of nanoparticles, J. Phys. Chem. C 112 (2008) 5715–5723, https://doi.org/10.1021/jp709667u.
60. S. Bhattacharjee, Review article DLS and zeta potential – what they are and what they are not?, J. Control. Release 235 (2016) 337–351, https://doi.org/10.1016/j.jconrel.2016.06.017.
61. H. Agarwal, A. Nakara, S. Menon, V. Shanmugam, Eco-friendly synthesis of zinc oxide nanoparticles using *Cinnamomum Tamala* leaf extract and its promising effect towards the antibacterial activity, J. Drug Deliv. Sci. Technol. 53 (2019) 101212, https://doi.org/10.1016/j.jddst.2019.101212.
62. K. Nithya, S. Kalyanasundharam, Effect of chemically synthesis compared to biosynthesized ZnO nanoparticles using aqueous extract of C. halicacabum and their antibacterial activity, OpenNano 4 (2019) 100024, https://doi.org/10.1016/j.onano.2018.10.001.
63. N. Vigneshwaran, S. Kumar, A.A. Kathe, P.V Varadarajan, V. Prasad, Functional finishing of cotton fabrics using zinc oxide-soluble starch nanocomposites, Nanotechnology 17 (2006) 5087–5095, https://doi.org/10.1088/0957-4484/17/20/008.
64. M.F. Cheira, M.N. Kouraim, I.H. Zidan, W.S. Mohamed, T.F. Hassanein, Adsorption of U(VI) from sulfate solution using montmorillonite/polyamide and nano-titanium oxide/polyamide nanocomposites, J. Environ. Chem. Eng. 8 (2020) 104427, https://doi.org/10.1016/j.jece.2020.104427.
65. T.F. Hassanein, A.M. Masoud, W.S. Mohamed, M.H. Taha, E. Guibal, Synthesis of polyamide 6/nano-hydroxyapatite hybrid (PA6/n-HAp) for the sorption of rare earth elements and uranium, J. Environ. Chem. Eng. 9 (2021) 104731, https://doi.org/10.1016/j.jece.2020.104731.
66. S. Mourdikoudis, R.M. Pallares, N.T K. Thanh, Characterization techniques for nanoparticles: comparison and complementarity upon studying nanoparticle properties, Nanoscale 10 (2018) 12871, https://doi.org/ 10.1039/c8nr02278j.
67. J. Lim, S.P. Yeap, H.X. Che, S.C. Low, Characterization of magnetic nanoparticle by dynamic light scattering, Nanoscale Res. Lett. 8 (2013) 381, https://doi.org/10.1186/1556-276X-8-381.
68. E.A.S. Dimapilis, C. Hsu, R.M.O. Mendoza, M. Lu, Zinc oxide nanoparticles for water disinfection, Sustain. Environ. Res. 28 (2018) 47-56, https://doi.org/10.1016/j.serj.2017.10.001.
69. P.K. Stoimenov, R.L. Klinger, G.L. Marchin, K.J. Klabunde, Metal oxide nanoparticles as

bactericidal agents, Langmuir 18 (2002) 6679-6686, https://doi.org/10.1021/la0202374.
70. L.L. Zhang, B. Chen, L.L. Xie, Z.F. Li, Study on the antimicrobial properties of ZnO suspension against Gram-positive and Gram-negative bacteria strains, Adv. Mater. Res. 393-395 (2011) 1488-1491, https://doi.org/10.4028/www.scientific.net/AMR.393-395.1488.
71. A.M. El Saeed, M.A. El- Fattah, A.M. Azzam, Synthesis of ZnO nanoparticles and studying its influence on the antimicrobial, anticorrosion and mechanical behavior of polyurethane composite for surface coating, Dyes Pigm. 121 (2015) 282-289, https://doi.org/10.1016/j.dyepig.2015.05.037.
72. F. Elmi, H. Alinezhad, Z. Moulana, F. Salehian, S.M. Tavakkoli, F. Asgharpour, H. Fallah, M.M. Elmi, The use of antibacterial activity of ZnO nanoparticles in the treatment of municipal wastewater, Water Sci. Technol. 70 (2014) 763-770, https://doi.org/10.2166/wst.2014.232.
73. A.A. Tayel, W.F. El-Tras, S. Moussa, A.F. El-Baz, H. Mahrous, M.F. Salem, L. Brimer, Antibacterial action of zinc oxide nanoparticles against foodborne pathogens, J. Food Saf. 31 (2011) 211-218, https://doi.org/10.1111/j.1745-4565.2010.00287.x.
74. J. Jayabalan, G. Mani, N. Krishnan, J. Pernabas, J.M. Devadoss, H.T. Jang, Green biogenic synthesis of zinc oxide nanoparticles using *Pseudomonas putida* culture and its *in vitro* antibacterial and anti-biofilm activity, Biocatal. Agric. Biotechnol. 21 (2019) 101327, https://doi.org/10.1016/j.bcab.2019.101327.
75. E. Zare, S. Pourseyedi, M. Khatami, E. Darezereshki, Simple biosynthesis of zinc oxide nanoparticles using nature's source, and it's *in vitro* bio-activity. J. Mol. Struct. 1146 (2017) 96-103, https://doi.org/10.1016/j.molstruc.2017.05.118.
76. M. Ganesh, S.G. Lee, J. Jayaprakash, M. Mohankumar, H.T. Jang, *Hydnocarpus alpina Wt* extract mediated green synthesis of ZnO nanoparticle and screening of its anti-microbial, free radical scavenging, and photocatalytic activity, Biocatal. Agri. Biotechnol. 19 (2019) 101129, https://doi.org/10.1016/j.bcab.2019.101129.
77. A. Sirelkhatim, S. Mahmud, A. Seeni, N.H.M. Kaus, L.C. Ann, S.K.M. Bakhori, H. Hasan, D. Mohamad, Review on zinc oxide nanoparticles: antibacterial activity and toxicity mechanism, Nano-Micro Lett. 7 (2015) 219-242, https://doi.org/10.1007/s40820-015-0040-x.
78. H.M.H. Al-Kordy, S.A. Sabry, M.E.M. Mabrouk, Photocatalytic and antimicrobial activity of zinc oxide nanoparticles synthesized by halophilic *Alkalibacillus* sp. w7 isolated from a salt lake, Egypt. J. Aquat. Biol. Fish. 24 (2020) 43-56, https://doi.org/10.21608/EJABF.2020.94732.
79. K.V. Dhandapani, D. Anbumani, A.D. Gandhi, P. Annamalai, B.S. Muthuvenkatachalam, P. Kavitha, B. Ranganathan, Green route for the synthesis of zinc oxide nanoparticles from *Melia azedarach* leaf extract and evaluation of their antioxidant and antibacterial activities, Biocatal. Agri. Biotechnol. 24 (2020) 101517, https://doi.org/10.1016/j.bcab.2020.101517.
80. S. Jiang, K. Lin, M. Cai, ZnO nanomaterials: current advancements in antibacterial mechanisms and applications, Front. Chem. 8 (2020) 580, https://doi.org/10.3389/fchem.2020.00580.
81. M.G. Demissie, F.K. Sabir, G.D. Edossa, B.A. Gonfa, Synthesis of zinc oxide nanoparticles using leaf extract of *Lippia adoensis* (Koseret) and evaluation of its antibacterial activity, J. chem. (2020) 7459042, https://doi.org/10.1155/2020/7459042.
82. A. Joe, S. Park, K. Shim, D. Kim, K. Jhee, H. Lee, C. Heo, H. Kim, E. Jang, Antibacterial mechanism of ZnO nanoparticles under dark conditions, J. Indus. Eng. Chem. 45 (2017) 430–439, https://doi.org/10.1016/j.jiec.2016.10.013.
83. R. Kumar, A. Umar, G. Kumar, H.S. Nalwa, Antimicrobial properties of ZnO nanomaterials: a review, Ceramics Intern. 43 (2017) 3940–3961, https://doi.org/10.1016/j.ceramint.2016.12.062.
84. S. Soren, S. Kumar, S. Mishra, P.K Jena, S.K Verma, P. Parhi, Evaluation of antibacterial and antioxidant potential of the zinc oxide nanoparticles synthesized by aqueous and polyol method, Microb. Pathog. 90 (2018) 78–84, https://doi.org/10.1016/j.micpath.2018.03.048.
85. H. Agarwal, S. Menon, S.V. Kumar, S. Rajeshkumar, Mechanistic study on antibacterial action of zinc oxide nanoparticles synthesized using green route, Chem.-Biol. Interact. 286 (2018) 60–70, https://doi.org/10.1016/j.cbi.2018.03.008.
86. L. Wang, C. Hu, L. Shao, The antimicrobial activity of nanoparticles: present situation and prospects for the future, Int. J. Nanomed. 12 (2017) 1227-1249, https://doi.org/10.2147/IJN.S121956.
87. M. Heinlaan, A. Ivask, I. Blinova, H.C. Dubourguier, A. Kahru, Toxicity of nanosized and bulk ZnO, CuO and TiO2 to bacteria *Vibrio fischeri* and crustaceans *Daphnia* magna and *Thamnocephalus platyurus*, Chemosphere 71

(2008) 1308-1316, https://doi.org/10.1016/j.chemosphere.2007.11.047.
88. C. Jayaseelan, A.A. Rahuman, A.V. Kirthi, S. Marimuthu, T. Santhoshkumar, A. Bagavan, K. Gaurav, L. Karthik, K.V.B. Rao, Novel microbial route to synthesize ZnO nanoparticles using *Aeromonas hydrophila* and their activity against pathogenic bacteria and fungi, Spectrochim. Acta A Mol. Biomol. Spectrosc. 90 (2012) 78–84, https://doi.org/10.1016/j.saa.2012.01.006.
89. R. Brayner, R. Ferrari-Iliou, N. Brivois, S. Djediat, M.F. Benedetti, F. Fievet, Toxicological impact studies based on *Escherichia coli* bacteria in ultrafine ZnO nanoparticles colloidal medium, Nano Lett. 6 (2006) 866-870, https://doi.org/10.1021/nl052326h.
90. C. Katepetch, R. Rujiravanit, H. Tamura, Formation of nanocrystalline ZnO particles into bacterial cellulose pellicle by ultrasonic-assisted in situ synthesis, Cellulose 20 (2013) 1275-1292, https://doi.org/10.1007/s10570-013-9892-8.
91. M. Yadollahi, I. Gholamali, H. Namazi, M. Aghazadeh, Synthesis and characterization of antibacterial carboxymethyl cellulose/ZnO nanocomposite hydrogels, Int. J. Biol. Macromol. 74 (2015) 136-141, https://doi.org/10.1016/j.ijbiomac.2014.11.032.
92. R.B. d'Água, R. Branquinho, M.P. Duarte, E. Maurício, A.L. Fernando, R. Martins, E. Fortunato, Efficient coverage of ZnO nanoparticles on cotton fibres for antibacterial finishing using a rapid and low cost in situ synthesis, New J. Chem. 42 (2018) 1052-1060, https://doi.org/10.1039/C7NJ03418K.
93. M.F. Elkady, H.H. Shokry, E.E. Hafez, A. Fouad, Construction of zinc oxide into different morphological structures to be utilized as antimicrobial agent against multidrug resistant bacteria, Bioinorg. Chem. Appl. 2015 (2015) 536854, https://doi.org/10.1155/2015/536854.
94. H.M. Yusof, N.A. Rahman, R. Mohamad, U.H. Zaidan, A.A. Samsudin, Biosynthesis of zinc oxide nanoparticles by cell-biomass and supernatant of *Lactobacillus plantarum* TA4 and its antibacterial and biocompatibility properties, Sci. Rep. 10 (2020) 19996, https://doi.org/10.1038/s41598-020-76402-w.
95. S.M.A Sharaf, S.E. Talat, G.E.M. Salem, H.A.M. Hendawy, , Antibacterial activities of sol-gel method synthesized zinc oxide nanoparticles against some resistant food-borne bacterial species, N. Egypt. J. Microbiol. 52 (2019).
96. F. Rubab, M.F. Chaudhary, N.M. Butt, Antibacterial effect of zinc oxide nanoparticles against water borne bacteria, TechConnect Briefs (2015) 344-348.
97. R.J. Barnes, R. Molina, J. Xu, P.J. Dobson, I.P. Thompson, Comparison of TiO_2 and ZnO nanoparticles for photocatalytic degradation of methylene blue and the correlated inactivation of gram-positive and gram-negative bacteria, J. Nanopart. Res. 15 (2013) 1432, https://doi.org/10.1007/s11051-013-1432-9.